Narrow-band search for gravitational waves from known pulsars using the second LIGO observing run

B. P. Abbott,[1] R. Abbott,[1] T. D. Abbott,[2] S. Abraham,[3] F. Acernese,[4,5] K. Ackley,[6] C. Adams,[7] R. X. Adhikari,[1] V. B. Adya,[8,9] C. Affeldt,[8,9] M. Agathos,[10] K. Agatsuma,[11] N. Aggarwal,[12] O. D. Aguiar,[13] L. Aiello,[14,15] A. Ain,[3] P. Ajith,[16] G. Allen,[17] A. Allocca,[18,19] M. A. Aloy,[20] P. A. Altin,[21] A. Amato,[22] A. Ananyeva,[1] S. B. Anderson,[1] W. G. Anderson,[23] S. V. Angelova,[24] S. Antier,[25] S. Appert,[1] K. Arai,[1] M. C. Araya,[1] J. S. Areeda,[26] M. Arène,[27] N. Arnaud,[25,28] S. Ascenzi,[29,30] G. Ashton,[6] S. M. Aston,[7] P. Astone,[31] F. Aubin,[32] P. Aufmuth,[9] K. AultONeal,[33] C. Austin,[2] V. Avendano,[34] A. Avila-Alvarez,[26] S. Babak,[35,27] P. Bacon,[27] F. Badaracco,[14,15] M. K. M. Bader,[36] S. Bae,[37] P. T. Baker,[38] F. Baldaccini,[39,40] G. Ballardin,[28] S. W. Ballmer,[41] S. Banagiri,[42] J. C. Barayoga,[1] S. E. Barclay,[43] B. C. Barish,[1] D. Barker,[44] K. Barkett,[45] S. Barnum,[12] F. Barone,[4,5] B. Barr,[43] L. Barsotti,[12] M. Barsuglia,[27] D. Barta,[46] J. Bartlett,[44] I. Bartos,[47] R. Bassiri,[48] A. Basti,[18,19] M. Bawaj,[49,40] J. C. Bayley,[43] M. Bazzan,[50,51] B. Bécsy,[52] M. Bejger,[27,53] I. Belahcene,[25] A. S. Bell,[43] D. Beniwal,[54] B. K. Berger,[48] G. Bergmann,[8,9] S. Bernuzzi,[55,56] J. J. Bero,[57] C. P. L. Berry,[58] D. Bersanetti,[59] A. Bertolini,[36] J. Betzwieser,[7] R. Bhandare,[60] J. Bidler,[26] I. A. Bilenko,[61] S. A. Bilgili,[38] G. Billingsley,[1] J. Birch,[7] R. Birney,[24] O. Birnholtz,[57] S. Biscans,[1,12] S. Biscoveanu,[6] A. Bisht,[9] M. Bitossi,[28,19] M. A. Bizouard,[25] J. K. Blackburn,[1] C. D. Blair,[7] D. G. Blair,[62] R. M. Blair,[44] S. Bloemen,[63] N. Bode,[8,9] M. Boer,[64] Y. Boetzel,[65] G. Bogaert,[64] F. Bondu,[66] E. Bonilla,[48] R. Bonnand,[32] P. Booker,[8,9] B. A. Boom,[36] C. D. Booth,[67] R. Bork,[1] V. Boschi,[28] S. Bose,[68,3] K. Bossie,[7] V. Bossilkov,[62] J. Bosveld,[62] Y. Bouffanais,[27] A. Bozzi,[28] C. Bradaschia,[19] P. R. Brady,[23] A. Bramley,[7] M. Branchesi,[14,15] J. E. Brau,[69] T. Briant,[70] J. H. Briggs,[43] F. Brighenti,[71,72] A. Brillet,[64] M. Brinkmann,[8,9] V. Brisson,[25,*] P. Brockill,[23] A. F. Brooks,[1] D. D. Brown,[54] S. Brunett,[1] A. Buikema,[12] T. Bulik,[73] H. J. Bulten,[74,36] A. Buonanno,[35,75] D. Buskulic,[32] C. Buy,[27] R. L. Byer,[48] M. Cabero,[8,9] L. Cadonati,[76] G. Cagnoli,[22,77] C. Cahillane,[1] J. Calderón Bustillo,[6] T. A. Callister,[1] E. Calloni,[78,5] J. B. Camp,[79] W. A. Campbell,[6] M. Canepa,[80,59] K. C. Cannon,[81] H. Cao,[54] J. Cao,[82] E. Capocasa,[27] F. Carbognani,[28] S. Caride,[83] M. F. Carney,[58] G. Carullo,[18] J. Casanueva Diaz,[19] C. Casentini,[29,30] S. Caudill,[36] M. Cavaglià,[84] F. Cavalier,[25] R. Cavalieri,[28] G. Cella,[19] P. Cerdá-Durán,[20] G. Cerretani,[18,19] E. Cesarini,[85,30] O. Chaibi,[64] K. Chakravarti,[3] S. J. Chamberlin,[86] M. Chan,[43] S. Chao,[87] P. Charlton,[88] E. A. Chase,[58] E. Chassande-Mottin,[27] D. Chatterjee,[23] M. Chaturvedi,[60] B. D. Cheeseboro,[38] H. Y. Chen,[89] X. Chen,[62] Y. Chen,[45] H.-P. Cheng,[47] C. K. Cheong,[90] H. Y. Chia,[47] A. Chincarini,[59] A. Chiummo,[28] G. Cho,[91] H. S. Cho,[92] M. Cho,[75] N. Christensen,[64,93] Q. Chu,[62] S. Chua,[70] K. W. Chung,[90] S. Chung,[62] G. Ciani,[50,51] A. A. Ciobanu,[54] R. Ciolfi,[94,95] F. Cipriano,[64] A. Cirone,[80,59] F. Clara,[44] J. A. Clark,[76] P. Clearwater,[96] F. Cleva,[64] C. Cocchieri,[84] E. Coccia,[14,15] P.-F. Cohadon,[70] D. Cohen,[25] R. Colgan,[97] M. Colleoni,[98] C. G. Collette,[99] C. Collins,[11] L. R. Cominsky,[100] M. Constancio Jr.,[13] L. Conti,[51] S. J. Cooper,[11] P. Corban,[7] T. R. Corbitt,[2] I. Cordero-Carrión,[101] K. R. Corley,[97] N. Cornish,[52] A. Corsi,[83] S. Cortese,[28] C. A. Costa,[13] R. Cotesta,[35] M. W. Coughlin,[1] S. B. Coughlin,[67,58] J.-P. Coulon,[64] S. T. Countryman,[97] P. Couvares,[1] P. B. Covas,[98] E. E. Cowan,[76] D. M. Coward,[62] M. J. Cowart,[7] D. C. Coyne,[1] R. Coyne,[102] J. D. E. Creighton,[23] T. D. Creighton,[103] J. Cripe,[2] M. Croquette,[70] S. G. Crowder,[104] T. J. Cullen,[2] A. Cumming,[43] L. Cunningham,[43] E. Cuoco,[28] T. Dal Canton,[79] G. Dálya,[105] S. L. Danilishin,[8,9] S. D'Antonio,[30] K. Danzmann,[9,8] A. Dasgupta,[106] C. F. Da Silva Costa,[47] L. E. H. Datrier,[43] V. Dattilo,[28] I. Dave,[60] M. Davier,[25] D. Davis,[41] E. J. Daw,[107] D. DeBra,[48] M. Deenadayalan,[3] J. Degallaix,[22] M. De Laurentis,[78,5] S. Deléglise,[70] W. Del Pozzo,[18,19] L. M. DeMarchi,[58] N. Demos,[12] T. Dent,[8,9,108] R. De Pietri,[109,56] J. Derby,[26] R. De Rosa,[78,5] C. De Rossi,[22,28] R. DeSalvo,[110] O. de Varona,[8,9] S. Dhurandhar,[3] M. C. Díaz,[103] T. Dietrich,[36] L. Di Fiore,[5] M. Di Giovanni,[111,95] T. Di Girolamo,[78,5] A. Di Lieto,[18,19] B. Ding,[99] S. Di Pace,[112,31] I. Di Palma,[112,31] F. Di Renzo,[18,19] A. Dmitriev,[11] Z. Doctor,[89] F. Donovan,[12] K. L. Dooley,[67,84] S. Doravari,[8,9] I. Dorrington,[67] T. P. Downes,[23] M. Drago,[14,15] J. C. Driggers,[44] Z. Du,[82] J.-G. Ducoin,[25] P. Dupej,[43] S. E. Dwyer,[44] P. J. Easter,[6] T. B. Edo,[107] M. C. Edwards,[93] A. Effler,[7] P. Ehrens,[1] J. Eichholz,[1] S. S. Eikenberry,[47] M. Eisenmann,[32] R. A. Eisenstein,[12] R. C. Essick,[89] H. Estelles,[98] D. Estevez,[32] Z. B. Etienne,[38] T. Etzel,[1] M. Evans,[12] T. M. Evans,[7] V. Fafone,[29,30,14] H. Fair,[41] S. Fairhurst,[67] X. Fan,[82] S. Farinon,[59] B. Farr,[69] W. M. Farr,[11] E. J. Fauchon-Jones,[67] M. Favata,[34] M. Fays,[107] M. Fazio,[113] C. Fee,[114] J. Feicht,[1] M. M. Fejer,[48] F. Feng,[27] A. Fernandez-Galiana,[12] I. Ferrante,[18,19] E. C. Ferreira,[13] T. A. Ferreira,[13] F. Ferrini,[28] F. Fidecaro,[18,19] I. Fiori,[28] D. Fiorucci,[27] M. Fishbach,[89] R. P. Fisher,[41,115] J. M. Fishner,[12] M. Fitz-Axen,[42] R. Flaminio,[32,116] M. Fletcher,[43] E. Flynn,[26] H. Fong,[117] J. A. Font,[20,118] P. W. F. Forsyth,[21] J.-D. Fournier,[64] S. Frasca,[112,31] F. Frasconi,[19] Z. Frei,[105] A. Freise,[11] R. Frey,[69] V. Frey,[25] P. Fritschel,[12] V. V. Frolov,[7] P. Fulda,[47] M. Fyffe,[7] H. A. Gabbard,[43]

B. U. Gadre,[3] S. M. Gaebel,[11] J. R. Gair,[119] L. Gammaitoni,[39] M. R. Ganija,[54] S. G. Gaonkar,[3] A. Garcia,[26] C. García-Quirós,[98] F. Garufi,[78, 5] B. Gateley,[44] S. Gaudio,[33] G. Gaur,[120] V. Gayathri,[121] G. Gemme,[59] E. Genin,[28] A. Gennai,[19] D. George,[17] J. George,[60] L. Gergely,[122] V. Germain,[32] S. Ghonge,[76] Abhirup Ghosh,[16] Archisman Ghosh,[36] S. Ghosh,[23] B. Giacomazzo,[111, 95] J. A. Giaime,[2, 7] K. D. Giardina,[7] A. Giazotto,[19, †] K. Gill,[33] G. Giordano,[4, 5] L. Glover,[110] P. Godwin,[86] E. Goetz,[44] R. Goetz,[47] B. Goncharov,[6] G. González,[2] J. M. Gonzalez Castro,[18, 19] A. Gopakumar,[123] M. L. Gorodetsky,[61] S. E. Gossan,[1] M. Gosselin,[28] R. Gouaty,[32] A. Grado,[124, 5] C. Graef,[43] M. Granata,[22] A. Grant,[43] S. Gras,[12] P. Grassia,[1] C. Gray,[44] R. Gray,[43] G. Greco,[71, 72] A. C. Green,[11, 47] R. Green,[67] E. M. Gretarsson,[33] P. Groot,[63] H. Grote,[67] S. Grunewald,[35] P. Gruning,[25] G. M. Guidi,[71, 72] H. K. Gulati,[106] Y. Guo,[36] A. Gupta,[86] M. K. Gupta,[106] E. K. Gustafson,[1] R. Gustafson,[125] L. Haegel,[98] O. Halim,[15, 14] B. R. Hall,[68] E. D. Hall,[12] E. Z. Hamilton,[67] G. Hammond,[43] M. Haney,[65] M. M. Hanke,[8, 9] J. Hanks,[44] C. Hanna,[86] O. A. Hannuksela,[90] J. Hanson,[7] T. Hardwick,[2] K. Haris,[16] J. Harms,[14, 15] G. M. Harry,[126] I. W. Harry,[35] C.-J. Haster,[117] K. Haughian,[43] F. J. Hayes,[43] J. Healy,[57] A. Heidmann,[70] M. C. Heintze,[7] H. Heitmann,[64] P. Hello,[25] G. Hemming,[28] M. Hendry,[43] I. S. Heng,[43] J. Hennig,[8, 9] A. W. Heptonstall,[1] Francisco Hernandez Vivanco,[6] M. Heurs,[8, 9] S. Hild,[43] T. Hinderer,[127, 36, 128] D. Hoak,[28] S. Hochheim,[8, 9] D. Hofman,[22] A. M. Holgado,[17] N. A. Holland,[21] K. Holt,[7] D. E. Holz,[89] P. Hopkins,[67] C. Horst,[23] J. Hough,[43] E. J. Howell,[62] C. G. Hoy,[67] A. Hreibi,[64] E. A. Huerta,[17] D. Huet,[25] B. Hughey,[33] M. Hulko,[1] S. Husa,[98] S. H. Huttner,[43] T. Huynh-Dinh,[7] B. Idzkowski,[73] A. Iess,[29, 30] C. Ingram,[54] R. Inta,[83] G. Intini,[112, 31] B. Irwin,[114] H. N. Isa,[43] J.-M. Isac,[70] M. Isi,[1] B. R. Iyer,[16] K. Izumi,[44] T. Jacqmin,[70] S. J. Jadhav,[129] K. Jani,[76] N. N. Janthalur,[129] P. Jaranowski,[130] A. C. Jenkins,[131] J. Jiang,[47] D. S. Johnson,[17] A. W. Jones,[11] D. I. Jones,[132] R. Jones,[43] R. J. G. Jonker,[36] L. Ju,[62] J. Junker,[8, 9] C. V. Kalaghatgi,[67] V. Kalogera,[58] B. Kamai,[1] S. Kandhasamy,[84] G. Kang,[37] J. B. Kanner,[1] S. J. Kapadia,[23] S. Karki,[69] K. S. Karvinen,[8, 9] R. Kashyap,[16] M. Kasprzack,[1] S. Katsanevas,[28] E. Katsavounidis,[12] W. Katzman,[7] S. Kaufer,[9] K. Kawabe,[44] N. V. Keerthana,[3] F. Kéfélian,[64] D. Keitel,[43] R. Kennedy,[107] J. S. Key,[133] F. Y. Khalili,[61] H. Khan,[26] I. Khan,[14, 30] S. Khan,[8, 9] Z. Khan,[106] E. A. Khazanov,[134] M. Khursheed,[60] N. Kijbunchoo,[21] Chunglee Kim,[135] J. C. Kim,[136] K. Kim,[90] W. Kim,[54] W. S. Kim,[137] Y.-M. Kim,[138] C. Kimball,[58] E. J. King,[54] P. J. King,[44] M. Kinley-Hanlon,[126] R. Kirchhoff,[8, 9] J. S. Kissel,[44] L. Kleybolte,[139] J. H. Klika,[23] S. Klimenko,[47] T. D. Knowles,[38] P. Koch,[8, 9] S. M. Koehlenbeck,[8, 9] G. Koekoek,[36, 140] S. Koley,[36] V. Kondrashov,[1] A. Kontos,[12] N. Koper,[8, 9] M. Korobko,[139] W. Z. Korth,[1] I. Kowalska,[73] D. B. Kozak,[1] V. Kringel,[8, 9] N. Krishnendu,[141] A. Królak,[142, 143] G. Kuehn,[8, 9] A. Kumar,[129] P. Kumar,[144] R. Kumar,[106] S. Kumar,[16] L. Kuo,[87] A. Kutynia,[142] S. Kwang,[23] B. D. Lackey,[35] K. H. Lai,[90] T. L. Lam,[90] M. Landry,[44] B. B. Lane,[12] R. N. Lang,[145] J. Lange,[57] B. Lantz,[48] R. K. Lanza,[12] A. Lartaux-Vollard,[25] P. D. Lasky,[6] M. Laxen,[7] A. Lazzarini,[1] C. Lazzaro,[51] P. Leaci,[112, 31] S. Leavey,[8, 9] Y. K. Lecoeuche,[44] C. H. Lee,[92] H. K. Lee,[146] H. M. Lee,[147] H. W. Lee,[136] J. Lee,[91] K. Lee,[43] J. Lehmann,[8, 9] A. Lenon,[38] N. Leroy,[25] N. Letendre,[32] Y. Levin,[6, 97] J. Li,[82] K. J. L. Li,[90] T. G. F. Li,[90] X. Li,[45] F. Lin,[6] F. Linde,[36] S. D. Linker,[110] T. B. Littenberg,[148] J. Liu,[62] X. Liu,[23] R. K. L. Lo,[90, 1] N. A. Lockerbie,[24] L. T. London,[67] A. Longo,[149, 150] M. Lorenzini,[14, 15] V. Loriette,[151] M. Lormand,[7] G. Losurdo,[19] J. D. Lough,[8, 9] G. Lovelace,[26] M. E. Lower,[152] H. Lück,[9, 8] D. Lumaca,[29, 30] A. P. Lundgren,[153] R. Lynch,[12] Y. Ma,[45] R. Macas,[67] S. Macfoy,[24] M. MacInnis,[12] D. M. Macleod,[67] A. Macquet,[64] F. Magaña-Sandoval,[41] L. Magaña Zertuche,[84] R. M. Magee,[86] E. Majorana,[31] I. Maksimovic,[151] A. Malik,[60] N. Man,[64] V. Mandic,[42] V. Mangano,[43] G. L. Mansell,[44, 12] M. Manske,[23, 21] M. Mantovani,[28] F. Marchesoni,[49, 40] F. Marion,[32] S. Márka,[97] Z. Márka,[97] C. Markakis,[10, 17] A. S. Markosyan,[48] A. Markowitz,[1] E. Maros,[1] A. Marquina,[101] S. Marsat,[35] F. Martelli,[71, 72] I. W. Martin,[43] R. M. Martin,[34] D. V. Martynov,[11] K. Mason,[12] E. Massera,[107] A. Masserot,[32] T. J. Massinger,[1] M. Masso-Reid,[43] S. Mastrogiovanni,[112, 31] A. Matas,[42, 35] F. Matichard,[1, 12] L. Matone,[97] N. Mavalvala,[12] N. Mazumder,[68] J. J. McCann,[62] R. McCarthy,[44] D. E. McClelland,[21] S. McCormick,[7] L. McCuller,[12] S. C. McGuire,[154] J. McIver,[1] D. J. McManus,[21] T. McRae,[21] S. T. McWilliams,[38] D. Meacher,[86] G. D. Meadors,[6] M. Mehmet,[8, 9] A. K. Mehta,[16] J. Meidam,[36] A. Melatos,[96] G. Mendell,[44] R. A. Mercer,[23] L. Mereni,[22] E. L. Merilh,[44] M. Merzougui,[64] S. Meshkov,[1] C. Messenger,[43] C. Messick,[86] R. Metzdorff,[70] P. M. Meyers,[96] H. Miao,[11] C. Michel,[22] H. Middleton,[96] E. E. Mikhailov,[155] L. Milano,[78, 5] A. L. Miller,[47] A. Miller,[112, 31] M. Millhouse,[52] J. C. Mills,[67] M. C. Milovich-Goff,[110] O. Minazzoli,[64, 156] Y. Minenkov,[30] A. Mishkin,[47] C. Mishra,[157] T. Mistry,[107] S. Mitra,[3] V. P. Mitrofanov,[61] G. Mitselmakher,[47] R. Mittleman,[12] G. Mo,[93] D. Moffa,[114] K. Mogushi,[84] S. R. P. Mohapatra,[12] M. Montani,[71, 72] C. J. Moore,[10] D. Moraru,[44] G. Moreno,[44] S. Morisaki,[81] B. Mours,[32] C. M. Mow-Lowry,[11] Arunava Mukherjee,[8, 9] D. Mukherjee,[23] S. Mukherjee,[103] N. Mukund,[3] A. Mullavey,[7] J. Munch,[54] E. A. Muñiz,[41] M. Muratore,[33] P. G. Murray,[43, 158, 159] I. Nardecchia,[29, 30] L. Naticchioni,[112, 31] R. K. Nayak,[160] J. Neilson,[110] G. Nelemans,[63, 36] T. J. N. Nelson,[7] M. Nery,[8, 9] A. Neunzert,[125] K. Y. Ng,[12] S. Ng,[54]

P. Nguyen,[69] D. Nichols,[127, 36] S. Nissanke,[127, 36] F. Nocera,[28] C. North,[67] L. K. Nuttall,[153] M. Obergaulinger,[20] J. Oberling,[44] B. D. O'Brien,[47] G. D. O'Dea,[110] G. H. Ogin,[161] J. J. Oh,[137] S. H. Oh,[137] F. Ohme,[8, 9] H. Ohta,[81] M. A. Okada,[13] M. Oliver,[98] P. Oppermann,[8, 9] Richard J. Oram,[7] B. O'Reilly,[7] R. G. Ormiston,[42] L. F. Ortega,[47] R. O'Shaughnessy,[57] S. Ossokine,[35] D. J. Ottaway,[54] H. Overmier,[7] B. J. Owen,[83] A. E. Pace,[86] G. Pagano,[18, 19] M. A. Page,[62] A. Pai,[121] S. A. Pai,[60] J. R. Palamos,[69] O. Palashov,[134] C. Palomba,[31] A. Pal-Singh,[139] Huang-Wei Pan,[87] B. Pang,[45] P. T. H. Pang,[90] C. Pankow,[58] F. Pannarale,[112, 31] B. C. Pant,[60] F. Paoletti,[19] A. Paoli,[28] A. Parida,[3] W. Parker,[7, 154] D. Pascucci,[43] A. Pasqualetti,[28] R. Passaquieti,[18, 19] D. Passuello,[19] M. Patil,[143] B. Patricelli,[18, 19] B. L. Pearlstone,[43] C. Pedersen,[67] M. Pedraza,[1] R. Pedurand,[22, 162] A. Pele,[7] S. Penn,[163] C. J. Perez,[44] A. Perreca,[111, 95] H. P. Pfeiffer,[35, 117] M. Phelps,[8, 9] K. S. Phukon,[3] O. J. Piccinni,[112, 31] M. Pichot,[64] F. Piergiovanni,[71, 72] G. Pillant,[28] L. Pinard,[22] M. Pirello,[44] M. Pitkin,[43] R. Poggiani,[18, 19] D. Y. T. Pong,[90] S. Ponrathnam,[3] P. Popolizio,[28] E. K. Porter,[27] J. Powell,[152] A. K. Prajapati,[106] J. Prasad,[3] K. Prasai,[48] R. Prasanna,[129] G. Pratten,[98] T. Prestegard,[23] S. Privitera,[35] G. A. Prodi,[111, 95] L. G. Prokhorov,[61] O. Puncken,[8, 9] M. Punturo,[40] P. Puppo,[31] M. Pürrer,[35] H. Qi,[23] V. Quetschke,[103] P. J. Quinonez,[33] E. A. Quintero,[1] R. Quitzow-James,[69] F. J. Raab,[44] H. Radkins,[44] N. Radulescu,[64] P. Raffai,[105] S. Raja,[60] C. Rajan,[60] B. Rajbhandari,[83] M. Rakhmanov,[103] K. E. Ramirez,[103] A. Ramos-Buades,[98] Javed Rana,[3] K. Rao,[58] P. Rapagnani,[112, 31] V. Raymond,[67] M. Razzano,[18, 19] J. Read,[26] T. Regimbau,[32] L. Rei,[59] S. Reid,[24] D. H. Reitze,[1, 47] W. Ren,[17] F. Ricci,[112, 31] C. J. Richardson,[33] J. W. Richardson,[1] P. M. Ricker,[17] K. Riles,[125] M. Rizzo,[58] N. A. Robertson,[1, 43] R. Robie,[43] F. Robinet,[25] A. Rocchi,[30] L. Rolland,[32] J. G. Rollins,[1] V. J. Roma,[69] M. Romanelli,[66] R. Romano,[4, 5] C. L. Romel,[44] J. H. Romie,[7] K. Rose,[114] D. Rosińska,[164, 53] S. G. Rosofsky,[17] M. P. Ross,[165] S. Rowan,[43] A. Rüdiger,[8, 9, ‡] P. Ruggi,[28] G. Rutins,[166] K. Ryan,[44] S. Sachdev,[1] T. Sadecki,[44] M. Sakellariadou,[131] L. Salconi,[28] M. Saleem,[141] A. Samajdar,[36] L. Sammut,[6] E. J. Sanchez,[1] L. E. Sanchez,[1] N. Sanchis-Gual,[20] V. Sandberg,[44] J. R. Sanders,[41] K. A. Santiago,[34] N. Sarin,[6] B. Sassolas,[22, 67] P. R. Saulson,[41] O. Sauter,[125] R. L. Savage,[44] P. Schale,[69] M. Scheel,[45] J. Scheuer,[58] P. Schmidt,[63] R. Schnabel,[139] R. M. S. Schofield,[69] A. Schönbeck,[139] E. Schreiber,[8, 9] B. W. Schulte,[8, 9] B. F. Schutz,[67] S. G. Schwalbe,[33] J. Scott,[43] S. M. Scott,[21] E. Seidel,[17] D. Sellers,[7] A. S. Sengupta,[167] N. Sennett,[35] D. Sentenac,[28] V. Sequino,[29, 30, 14] A. Sergeev,[134] Y. Setyawati,[8, 9] D. A. Shaddock,[21] T. Shaffer,[44] M. S. Shahriar,[58] M. B. Shaner,[110] L. Shao,[35] P. Sharma,[60] P. Shawhan,[75] H. Shen,[17] R. Shink,[168] D. H. Shoemaker,[12] D. M. Shoemaker,[76] S. ShyamSundar,[60] K. Siellez,[76] M. Sieniawska,[53] D. Sigg,[44] A. D. Silva,[13] L. P. Singer,[79] N. Singh,[73] A. Singhal,[14, 31] A. M. Sintes,[98] S. Sitmukhambetov,[103] V. Skliris,[67] B. J. J. Slagmolen,[21] T. J. Slaven-Blair,[62] J. R. Smith,[26] R. J. E. Smith,[6] S. Somala,[169] E. J. Son,[137] B. Sorazu,[43] F. Sorrentino,[59] T. Souradeep,[3] E. Sowell,[83] A. P. Spencer,[43] A. K. Srivastava,[106] V. Srivastava,[41] K. Staats,[58] C. Stachie,[64] M. Standke,[8, 9] D. A. Steer,[27] M. Steinke,[8, 9] J. Steinlechner,[139, 43] S. Steinlechner,[139] D. Steinmeyer,[8, 9] S. P. Stevenson,[152] D. Stocks,[48] R. Stone,[103] D. J. Stops,[11] K. A. Strain,[43] G. Stratta,[71, 72] S. E. Strigin,[61] A. Strunk,[44] R. Sturani,[170] A. L. Stuver,[171] V. Sudhir,[12] T. Z. Summerscales,[172] L. Sun,[1] S. Sunil,[106] J. Suresh,[3] P. J. Sutton,[67] B. L. Swinkels,[36] M. J. Szczepańczyk,[33] M. Tacca,[36] S. C. Tait,[43] C. Talbot,[6] D. Talukder,[69] D. B. Tanner,[47] M. Tápai,[122] A. Taracchini,[35] J. D. Tasson,[93] R. Taylor,[1] F. Thies,[8, 9] M. Thomas,[7] P. Thomas,[44] S. R. Thondapu,[60] K. A. Thorne,[7] E. Thrane,[6] Shubhanshu Tiwari,[111, 95] Srishti Tiwari,[123] V. Tiwari,[67] K. Toland,[43] M. Tonelli,[18, 19] Z. Tornasi,[43] A. Torres-Forné,[173] C. I. Torrie,[1] D. Töyrä,[11] F. Travasso,[28, 40] G. Traylor,[7] M. C. Tringali,[73] A. Trovato,[27] L. Trozzo,[174, 19] R. Trudeau,[1] K. W. Tsang,[36] M. Tse,[12] R. Tso,[45] L. Tsukada,[81] D. Tsuna,[81] D. Tuyenbayev,[103] K. Ueno,[81] D. Ugolini,[175] C. S. Unnikrishnan,[123] A. L. Urban,[2] S. A. Usman,[67] H. Vahlbruch,[9] G. Vajente,[1] G. Valdes,[2] N. van Bakel,[36] M. van Beuzekom,[36] J. F. J. van den Brand,[74, 36] C. Van Den Broeck,[36, 176] D. C. Vander-Hyde,[41] J. V. van Heijningen,[62] L. van der Schaaf,[36] A. A. van Veggel,[43] M. Vardaro,[50, 51] V. Varma,[45] S. Vass,[1] M. Vasúth,[46] A. Vecchio,[11] G. Vedovato,[51] J. Veitch,[43] P. J. Veitch,[54] K. Venkateswara,[165] G. Venugopalan,[1] D. Verkindt,[32] F. Vetrano,[71, 72] A. Viceré,[71, 72] A. D. Viets,[23] D. J. Vine,[166] J.-Y. Vinet,[64] S. Vitale,[12] T. Vo,[41] H. Vocca,[39, 40] C. Vorvick,[44] S. P. Vyatchanin,[61] A. R. Wade,[1] L. E. Wade,[114] M. Wade,[114] R. Walet,[36] M. Walker,[26] L. Wallace,[1] S. Walsh,[23] G. Wang,[14, 19] H. Wang,[11] J. Z. Wang,[125] W. H. Wang,[103] Y. F. Wang,[90] R. L. Ward,[21] Z. A. Warden,[33] J. Warner,[44] M. Was,[32] J. Watchi,[99] B. Weaver,[44] L.-W. Wei,[8, 9] M. Weinert,[8, 9] A. J. Weinstein,[1] R. Weiss,[12] F. Wellmann,[8, 9] L. Wen,[62] E. K. Wessel,[17] P. Weßels,[8, 9] J. W. Westhouse,[33] K. Wette,[21] J. T. Whelan,[57] B. F. Whiting,[47] C. Whittle,[12] D. M. Wilken,[8, 9] D. Williams,[43] A. R. Williamson,[127, 36] J. L. Willis,[1] B. Willke,[8, 9] M. H. Wimmer,[8, 9] W. Winkler,[8, 9] C. C. Wipf,[1] H. Wittel,[8, 9] G. Woan,[43] J. Woehler,[8, 9] J. K. Wofford,[57] J. Worden,[44] J. L. Wright,[43] D. S. Wu,[8, 9] D. M. Wysocki,[57] L. Xiao,[1] H. Yamamoto,[1] C. C. Yancey,[75] L. Yang,[113] M. J. Yap,[21] M. Yazback,[47] D. W. Yeeles,[67] Hang Yu,[12] Haocun Yu,[12] S. H. R. Yuen,[90] M. Yvert,[32] A. K. Zadrożny,[103, 142] M. Zanolin,[33] T. Zelenova,[28] J.-P. Zendri,[51] M. Zevin,[58]

J. Zhang,[62] L. Zhang,[1] T. Zhang,[43] C. Zhao,[62] M. Zhou,[58] Z. Zhou,[58] X. J. Zhu,[6] M. E. Zucker,[1, 12] and J. Zweizig[1]

(The LIGO Scientific Collaboration and the Virgo Collaboration)

M. Keith,[177] M. Kerr,[178] L. Kuiper,[179] A. K. Harding,[180]
A. Lyne,[177] J. Palfreyman,[181] B. Stappers,[177] and P. Weltervrede[177]

[1]*LIGO, California Institute of Technology, Pasadena, CA 91125, USA*
[2]*Louisiana State University, Baton Rouge, LA 70803, USA*
[3]*Inter-University Centre for Astronomy and Astrophysics, Pune 411007, India*
[4]*Università di Salerno, Fisciano, I-84084 Salerno, Italy*
[5]*INFN, Sezione di Napoli, Complesso Universitario di Monte S.Angelo, I-80126 Napoli, Italy*
[6]*OzGrav, School of Physics & Astronomy, Monash University, Clayton 3800, Victoria, Australia*
[7]*LIGO Livingston Observatory, Livingston, LA 70754, USA*
[8]*Max Planck Institute for Gravitational Physics (Albert Einstein Institute), D-30167 Hannover, Germany*
[9]*Leibniz Universität Hannover, D-30167 Hannover, Germany*
[10]*University of Cambridge, Cambridge CB2 1TN, United Kingdom*
[11]*University of Birmingham, Birmingham B15 2TT, United Kingdom*
[12]*LIGO, Massachusetts Institute of Technology, Cambridge, MA 02139, USA*
[13]*Instituto Nacional de Pesquisas Espaciais, 12227-010 São José dos Campos, São Paulo, Brazil*
[14]*Gran Sasso Science Institute (GSSI), I-67100 L'Aquila, Italy*
[15]*INFN, Laboratori Nazionali del Gran Sasso, I-67100 Assergi, Italy*
[16]*International Centre for Theoretical Sciences, Tata Institute of Fundamental Research, Bengaluru 560089, India*
[17]*NCSA, University of Illinois at Urbana-Champaign, Urbana, IL 61801, USA*
[18]*Università di Pisa, I-56127 Pisa, Italy*
[19]*INFN, Sezione di Pisa, I-56127 Pisa, Italy*
[20]*Departamento de Astronomía y Astrofísica, Universitat de València, E-46100 Burjassot, València, Spain*
[21]*OzGrav, Australian National University, Canberra, Australian Capital Territory 0200, Australia*
[22]*Laboratoire des Matériaux Avancés (LMA), CNRS/IN2P3, F-69622 Villeurbanne, France*
[23]*University of Wisconsin-Milwaukee, Milwaukee, WI 53201, USA*
[24]*SUPA, University of Strathclyde, Glasgow G1 1XQ, United Kingdom*
[25]*LAL, Univ. Paris-Sud, CNRS/IN2P3, Université Paris-Saclay, F-91898 Orsay, France*
[26]*California State University Fullerton, Fullerton, CA 92831, USA*
[27]*APC, AstroParticule et Cosmologie, Université Paris Diderot,*
CNRS/IN2P3, CEA/Irfu, Observatoire de Paris,
Sorbonne Paris Cité, F-75205 Paris Cedex 13, France
[28]*European Gravitational Observatory (EGO), I-56021 Cascina, Pisa, Italy*
[29]*Università di Roma Tor Vergata, I-00133 Roma, Italy*
[30]*INFN, Sezione di Roma Tor Vergata, I-00133 Roma, Italy*
[31]*INFN, Sezione di Roma, I-00185 Roma, Italy*
[32]*Laboratoire d'Annecy de Physique des Particules (LAPP), Univ. Grenoble Alpes,*
Université Savoie Mont Blanc, CNRS/IN2P3, F-74941 Annecy, France
[33]*Embry-Riddle Aeronautical University, Prescott, AZ 86301, USA*
[34]*Montclair State University, Montclair, NJ 07043, USA*
[35]*Max Planck Institute for Gravitational Physics (Albert Einstein Institute), D-14476 Potsdam-Golm, Germany*
[36]*Nikhef, Science Park 105, 1098 XG Amsterdam, The Netherlands*
[37]*Korea Institute of Science and Technology Information, Daejeon 34141, South Korea*
[38]*West Virginia University, Morgantown, WV 26506, USA*
[39]*Università di Perugia, I-06123 Perugia, Italy*
[40]*INFN, Sezione di Perugia, I-06123 Perugia, Italy*
[41]*Syracuse University, Syracuse, NY 13244, USA*
[42]*University of Minnesota, Minneapolis, MN 55455, USA*
[43]*SUPA, University of Glasgow, Glasgow G12 8QQ, United Kingdom*
[44]*LIGO Hanford Observatory, Richland, WA 99352, USA*
[45]*Caltech CaRT, Pasadena, CA 91125, USA*
[46]*Wigner RCP, RMKI, H-1121 Budapest, Konkoly Thege Miklós út 29-33, Hungary*
[47]*University of Florida, Gainesville, FL 32611, USA*
[48]*Stanford University, Stanford, CA 94305, USA*
[49]*Università di Camerino, Dipartimento di Fisica, I-62032 Camerino, Italy*
[50]*Università di Padova, Dipartimento di Fisica e Astronomia, I-35131 Padova, Italy*
[51]*INFN, Sezione di Padova, I-35131 Padova, Italy*
[52]*Montana State University, Bozeman, MT 59717, USA*
[53]*Nicolaus Copernicus Astronomical Center, Polish Academy of Sciences, 00-716, Warsaw, Poland*
[54]*OzGrav, University of Adelaide, Adelaide, South Australia 5005, Australia*

[55] *Theoretisch-Physikalisches Institut, Friedrich-Schiller-Universität Jena, D-07743 Jena, Germany*
[56] *INFN, Sezione di Milano Bicocca, Gruppo Collegato di Parma, I-43124 Parma, Italy*
[57] *Rochester Institute of Technology, Rochester, NY 14623, USA*
[58] *Center for Interdisciplinary Exploration & Research in Astrophysics (CIERA),*
Northwestern University, Evanston, IL 60208, USA
[59] *INFN, Sezione di Genova, I-16146 Genova, Italy*
[60] *RRCAT, Indore, Madhya Pradesh 452013, India*
[61] *Faculty of Physics, Lomonosov Moscow State University, Moscow 119991, Russia*
[62] *OzGrav, University of Western Australia, Crawley, Western Australia 6009, Australia*
[63] *Department of Astrophysics/IMAPP, Radboud University Nijmegen,*
P.O. Box 9010, 6500 GL Nijmegen, The Netherlands
[64] *Artemis, Université Côte d'Azur, Observatoire Côte d'Azur,*
CNRS, CS 34229, F-06304 Nice Cedex 4, France
[65] *Physik-Institut, University of Zurich, Winterthurerstrasse 190, 8057 Zurich, Switzerland*
[66] *Univ Rennes, CNRS, Institut FOTON - UMR6082, F-3500 Rennes, France*
[67] *Cardiff University, Cardiff CF24 3AA, United Kingdom*
[68] *Washington State University, Pullman, WA 99164, USA*
[69] *University of Oregon, Eugene, OR 97403, USA*
[70] *Laboratoire Kastler Brossel, Sorbonne Université, CNRS,*
ENS-Université PSL, Collège de France, F-75005 Paris, France
[71] *Università degli Studi di Urbino 'Carlo Bo,' I-61029 Urbino, Italy*
[72] *INFN, Sezione di Firenze, I-50019 Sesto Fiorentino, Firenze, Italy*
[73] *Astronomical Observatory Warsaw University, 00-478 Warsaw, Poland*
[74] *VU University Amsterdam, 1081 HV Amsterdam, The Netherlands*
[75] *University of Maryland, College Park, MD 20742, USA*
[76] *School of Physics, Georgia Institute of Technology, Atlanta, GA 30332, USA*
[77] *Université Claude Bernard Lyon 1, F-69622 Villeurbanne, France*
[78] *Università di Napoli 'Federico II,' Complesso Universitario di Monte S.Angelo, I-80126 Napoli, Italy*
[79] *NASA Goddard Space Flight Center, Greenbelt, MD 20771, USA*
[80] *Dipartimento di Fisica, Università degli Studi di Genova, I-16146 Genova, Italy*
[81] *RESCEU, University of Tokyo, Tokyo, 113-0033, Japan.*
[82] *Tsinghua University, Beijing 100084, China*
[83] *Texas Tech University, Lubbock, TX 79409, USA*
[84] *The University of Mississippi, University, MS 38677, USA*
[85] *Museo Storico della Fisica e Centro Studi e Ricerche "Enrico Fermi",*
I-00184 Roma, Italyrico Fermi, I-00184 Roma, Italy
[86] *The Pennsylvania State University, University Park, PA 16802, USA*
[87] *National Tsing Hua University, Hsinchu City, 30013 Taiwan, Republic of China*
[88] *Charles Sturt University, Wagga Wagga, New South Wales 2678, Australia*
[89] *University of Chicago, Chicago, IL 60637, USA*
[90] *The Chinese University of Hong Kong, Shatin, NT, Hong Kong*
[91] *Seoul National University, Seoul 08826, South Korea*
[92] *Pusan National University, Busan 46241, South Korea*
[93] *Carleton College, Northfield, MN 55057, USA*
[94] *INAF, Osservatorio Astronomico di Padova, I-35122 Padova, Italy*
[95] *INFN, Trento Institute for Fundamental Physics and Applications, I-38123 Povo, Trento, Italy*
[96] *OzGrav, University of Melbourne, Parkville, Victoria 3010, Australia*
[97] *Columbia University, New York, NY 10027, USA*
[98] *Universitat de les Illes Balears, IAC3—IEEC, E-07122 Palma de Mallorca, Spain*
[99] *Université Libre de Bruxelles, Brussels 1050, Belgium*
[100] *Sonoma State University, Rohnert Park, CA 94928, USA*
[101] *Departamento de Matemáticas, Universitat de València, E-46100 Burjassot, València, Spain*
[102] *University of Rhode Island, Kingston, RI 02881, USA*
[103] *The University of Texas Rio Grande Valley, Brownsville, TX 78520, USA*
[104] *Bellevue College, Bellevue, WA 98007, USA*
[105] *MTA-ELTE Astrophysics Research Group, Institute of Physics, Eötvös University, Budapest 1117, Hungary*
[106] *Institute for Plasma Research, Bhat, Gandhinagar 382428, India*
[107] *The University of Sheffield, Sheffield S10 2TN, United Kingdom*
[108] *IGFAE, Campus Sur, Universidade de Santiago de Compostela, 15782 Spain*
[109] *Dipartimento di Scienze Matematiche, Fisiche e Informatiche, Università di Parma, I-43124 Parma, Italy*
[110] *California State University, Los Angeles, 5151 State University Dr, Los Angeles, CA 90032, USA*
[111] *Università di Trento, Dipartimento di Fisica, I-38123 Povo, Trento, Italy*
[112] *Università di Roma 'La Sapienza,' I-00185 Roma, Italy*
[113] *Colorado State University, Fort Collins, CO 80523, USA*

[114]Kenyon College, Gambier, OH 43022, USA

[115]Christopher Newport University, Newport News, VA 23606, USA

[116]National Astronomical Observatory of Japan, 2-21-1 Osawa, Mitaka, Tokyo 181-8588, Japan

[117]Canadian Institute for Theoretical Astrophysics,
University of Toronto, Toronto, Ontario M5S 3H8, Canada

[118]Observatori Astronòmic, Universitat de València, E-46980 Paterna, València, Spain

[119]School of Mathematics, University of Edinburgh, Edinburgh EH9 3FD, United Kingdom

[120]Institute Of Advanced Research, Gandhinagar 382426, India

[121]Indian Institute of Technology Bombay, Powai, Mumbai 400 076, India

[122]University of Szeged, Dóm tér 9, Szeged 6720, Hungary

[123]Tata Institute of Fundamental Research, Mumbai 400005, India

[124]INAF, Osservatorio Astronomico di Capodimonte, I-80131, Napoli, Italy

[125]University of Michigan, Ann Arbor, MI 48109, USA

[126]American University, Washington, D.C. 20016, USA

[127]GRAPPA, Anton Pannekoek Institute for Astronomy and Institute of High-Energy Physics,
University of Amsterdam, Science Park 904, 1098 XH Amsterdam, The Netherlands

[128]Delta Institute for Theoretical Physics, Science Park 904, 1090 GL Amsterdam, The Netherlands

[129]Directorate of Construction, Services & Estate Management, Mumbai 400094 India

[130]University of Białystok, 15-424 Białystok, Poland

[131]King's College London, University of London, London WC2R 2LS, United Kingdom

[132]University of Southampton, Southampton SO17 1BJ, United Kingdom

[133]University of Washington Bothell, Bothell, WA 98011, USA

[134]Institute of Applied Physics, Nizhny Novgorod, 603950, Russia

[135]Ewha Womans University, Seoul 03760, South Korea

[136]Inje University Gimhae, South Gyeongsang 50834, South Korea

[137]National Institute for Mathematical Sciences, Daejeon 34047, South Korea

[138]Ulsan National Institute of Science and Technology, Ulsan 44919, South Korea

[139]Universität Hamburg, D-22761 Hamburg, Germany

[140]Maastricht University, P.O. Box 616, 6200 MD Maastricht, The Netherlands

[141]Chennai Mathematical Institute, Chennai 603103, India

[142]NCBJ, 05-400 Świerk-Otwock, Poland

[143]Institute of Mathematics, Polish Academy of Sciences, 00656 Warsaw, Poland

[144]Cornell University, Ithaca, NY 14850, USA

[145]Hillsdale College, Hillsdale, MI 49242, USA

[146]Hanyang University, Seoul 04763, South Korea

[147]Korea Astronomy and Space Science Institute, Daejeon 34055, South Korea

[148]NASA Marshall Space Flight Center, Huntsville, AL 35811, USA

[149]Dipartimento di Matematica e Fisica, Università degli Studi Roma Tre, I-00146 Roma, Italy

[150]INFN, Sezione di Roma Tre, I-00146 Roma, Italy

[151]ESPCI, CNRS, F-75005 Paris, France

[152]OzGrav, Swinburne University of Technology, Hawthorn VIC 3122, Australia

[153]University of Portsmouth, Portsmouth, PO1 3FX, United Kingdom

[154]Southern University and A&M College, Baton Rouge, LA 70813, USA

[155]College of William and Mary, Williamsburg, VA 23187, USA

[156]Centre Scientifique de Monaco, 8 quai Antoine Ier, MC-98000, Monaco

[157]Indian Institute of Technology Madras, Chennai 600036, India

[158]INFN Sezione di Torino, Via P. Giuria 1, I-10125 Torino, Italy

[159]Institut des Hautes Etudes Scientifiques, F-91440 Bures-sur-Yvette, France

[160]IISER-Kolkata, Mohanpur, West Bengal 741252, India

[161]Whitman College, 345 Boyer Avenue, Walla Walla, WA 99362 USA

[162]Université de Lyon, F-69361 Lyon, France

[163]Hobart and William Smith Colleges, Geneva, NY 14456, USA

[164]Janusz Gil Institute of Astronomy, University of Zielona Góra, 65-265 Zielona Góra, Poland

[165]University of Washington, Seattle, WA 98195, USA

[166]SUPA, University of the West of Scotland, Paisley PA1 2BE, United Kingdom

[167]Indian Institute of Technology, Gandhinagar Ahmedabad Gujarat 382424, India

[168]Université de Montréal/Polytechnique, Montreal, Quebec H3T 1J4, Canada

[169]Indian Institute of Technology Hyderabad, Sangareddy, Khandi, Telangana 502285, India

[170]International Institute of Physics, Universidade Federal do Rio Grande do Norte, Natal RN 59078-970, Brazil

[171]Villanova University, 800 Lancaster Ave, Villanova, PA 19085, USA

[172]Andrews University, Berrien Springs, MI 49104, USA

[173]Max Planck Institute for Gravitationalphysik (Albert Einstein Institute), D-14476 Potsdam-Golm, Germany

[174]Università di Siena, I-53100 Siena, Italy

[175]Trinity University, San Antonio, TX 78212, USA

[176] *Van Swinderen Institute for Particle Physics and Gravity,*
University of Groningen, Nijenborgh 4, 9747 AG Groningen, The Netherlands
[177] *School of Physics and Astronomy, University of Manchester, Manchester, M13 9PL, UK*
[178] *Space Science Division, Naval Research Laboratory, Washington, DC 20375-5352, USA*
[179] *SRON-Netherlands Institute for Space Research,*
Sorbonnelaan 2, NL-3584 CA Utrecht, Netherlands
[180] *Astrophysics Science Division, NASA Goddard Space Flight Center, Greenbelt, MD 20771, USA*
[181] *Department of Physical Sciences, University of Tasmania,*
Private Bag 37, Hobart, Tasmania 7001, Australia
(Dated: May 23, 2019)

Isolated spinning neutron stars, asymmetric with respect to their rotation axis, are expected to be sources of continuous gravitational waves. The most sensitive searches for these sources are based on accurate matched filtering techniques, that assume the continuous wave to be phase-locked with the pulsar beamed emission. While matched filtering maximizes the search sensitivity, a significant signal-to-noise ratio loss will happen in case of a mismatch between the assumed and the true signal phase evolution. Narrow-band algorithms allow for a small mismatch in the frequency and spin-down values of the pulsar while integrating coherently the entire data set. In this paper we describe a narrow-band search using LIGO O2 data for the continuous wave emission of 33 pulsars. No evidence for a continuous wave signal has been found and upper-limits on the gravitational wave amplitude, over the analyzed frequency and spin-down ranges, have been computed for each of the targets. In this search we have surpassed the spin-down limit, namely the maximum rotational energy loss due to gravitational waves emission, for some of the pulsars already present in the O1 LIGO narrow-band search, such as J1400−6325 J1813−1246, J1833−1034, J1952+3252, and for new targets such as J0940−5428 and J1747−2809. For J1400−6325, J1833−1034 and J1747−2809 this is the first time the spin-down limit is surpassed.

I. INTRODUCTION

Eleven gravitational wave (GW) signals have so far been detected by the LIGO [1, 2] and Virgo GW interferometers [3] in their first and second observing runs (O1 and O2, respectively) [4]. All the signals detected so far come from the coalescence of two compact objects. These signals belong to the class of *transient signals*, since they are observed only within a short time window during the observing run. Ten detection of binary black holes merger [4–9] and a detection from a binary neutron star (NS) merger [10] have been accomplished during the first and second observing runs.

Another class of GW signals potentially observable by the LIGO and Virgo detectors are the so-called *continuous wave* (CW). CWs could be potentially present during the entire data taking period of the GW detectors. Potential sources of CWs are isolated spinning NSs asymmetric with respect to their rotation axis. In the case of an oblate NS, CWs are emitted at a frequency of two times its rotational frequency.

Different types of CW searches can be performed according to the astrophysical scenario in which the NS is observed. If the NS is a pulsar, an accurate ephemeris may be available and matched filtering techniques can be employed to reach, ideally, the best possible sensitivity by using waveform templates that cover the entire observing run. These types of searches are referred as *tar-*

geted searches. The LIGO and Virgo Collaborations have already searched for this type of emission from known pulsars (both isolated and some in binaries) [11–19], for which accurate ephemerides were available. While for NSs observed as a central compact object of a supernova remnant or in a binary system, usually accurate ephemereides are not available. In this case we can pinpoint the source and look for the CW signal over a wide frequency range using semi-coherent analysis, e.g. dividing the observing run in several data chunks and looking for a waveform template in each of them. Such searches are called *"directed"* and offer the possibility to explore a large number of templates at the price of a lower sensitivity with respect to targeted searches[20–24]. Recently, there has been also a study for a possible deviation of CW signals from the General Relativity model[25], by including non-tensorial modes.

Between targeted and directed searches we find the *narrow-band* searches. Such pipelines are based on algorithms which allow to make a full coherent search and, at the same time, are able to deal with a frequency mismatch between the CW signal and the electromagnetic inferred value of the order of 500 mHz [14, 26, 27]. Usually, this will correspond to the evaluation of millions of waveform templates for each pulsar considered into the analysis.

Hence, narrow-band searches offers a sensitivity comparable to the one of targeted searches while relaxing the phase-lock assumption of the CW signal with the NS rotation. The CW phase-locking is indeed a strong assumption that may prevent the detection of a CW signal. In fact, a coherent (or targeted) CW search that uses 1 year of data has a frequency resolution of about

———

* Deceased, February 2018.
† Deceased, November 2017.
‡ Deceased, July 2018.

3×10^{-8} Hz. A mismatch between the rotational frequency inferred from the ephemeris and the CW signal frequency, of this size or larger, is enough to drastically reduce the chance of detection.

A small frequency mismatch may arise for several physical reasons, that usually are parametrized in a frequency mismatch of the form $\Delta f_{gw} \sim f_{gw}(1+\delta)$ [14]. In the case of a differential rotation between the GW engine and the electromagnetic pulse engine, the factor δ will be proportional to the timescale of some torque which enforces correlation between the two engines. Another possibility is that the NS is freely-precessing. In this scenario the δ factor will be proportional to the angle between the star symmetry axis and the star rotation axis [28]. In some of the previous narrow-band searches [14, 26] we used a value of $\delta \sim 10^{-4}$, which can accommodate the previous theoretical models. However starting from the first narrow-band search with advanced detector data [27], we explore a frequency/spin-down range corresponding to $\delta \sim 10^{-3}$.

Another possibility is that the pulsar ephemerides provided are not accurate enough to carry on targeted searches with the required resolution, or they are not available during the observing time of our detectors. That is the case for many low frequency and energetic pulsars observed in the X and γ-ray bands, such as J1833-1034 and J1813-1749. For these reasons, along with targeted searches, we search for CWs also with narrow-band searches.

In this paper we present the narrow-band search for CWs from 33 known pulsars using LIGO O2 data. In Sec. II we provide a brief background on the CW signal model and the algorithm used. In Sec. III we summarize the main features of the O2 narrow-band analysis, while in Sec. IV we introduce the pulsars that we have selected for this search. The results of the search, followed by the upper-limits on the signal strain amplitude, are discussed in Sec. V. Finally in Sec. VI we draw the conclusion of this work.

II. BACKGROUND

A. The signal

The GW signal emitted by an asymmetric spinning NS can be written at the detector frame, using the formalism introduced in [29], as the real part of

$$h(t) = H_0(H^+(\eta,\psi)A_+(t)+H^\times(\eta,\psi)A_\times(t))e^{2\pi i f_{gw}(t)t+i\phi_0} \tag{1}$$

where $f_{gw}(t)$ is the GW frequency (which incorporates all the modulation of the signal at the detector frame) and ϕ_0 an initial phase. The polarization amplitudes $H^+(\eta,\psi), H^\times(\eta,\psi)$ are functions of the ratio of the polarization ellipse semi-minor to semi-major axis η and the polarization angle ψ. The functions $A_+(t), A_\times(t)$ are the detector responses to the two wave polarizations. These two functions depend by the detector geographical location and the $0, \pm1, \pm2$ harmonics of the sidereal rotational frequency of the Earth F_{sid} (the inverse of the sidereal day), see [29] for more details. In Eq. (1), the amplitude of the GW H_0 is related to the canonical strain amplitude h_0 given the angle between the line of sight and the star rotation axis ι:

$$H_0 = h_0\sqrt{\frac{1 + 6\cos^2\iota + \cos^4\iota}{4}} \tag{2}$$

and

$$h_0 = \frac{1}{d}\frac{4\pi^2 G}{c^4}I_{zz}f_{gw}^2\epsilon. \tag{3}$$

Being d, I_{zz} and ϵ the star distance, moment of inertia with respect to the rotation axis and *ellipticity*. The ellipticity measures the degree of asymmetry of the star with respect to its rotation axis. In the detector reference frame the signal is modulated by several effects, the most important being the *Römer delay* (also called barycentric correction) due to the detector motion, given by the Earth's orbital motion and rotation, with respect to the GW source. Moreover the GW signal is also modulated by the source's intrinsic spin-down, due to the rotational energy loss from the source. Given a measure of the pulsar rotational frequency f_{rot}, its derivative $\dot{f}_{rot}$ and distance d, the GW signal amplitude can be constrained, assuming that all the star's rotational energy is lost via gravitational radiation. This theoretical value, which is an upper limit on the rotational energy that can be emitted in GWs, is called *spin-down limit* and is given by [30]:

$$h_{sd} = 8.06 \times 10^{-19}I_{38}^{1/2}\left[\frac{1\text{kpc}}{d}\right]\left[\frac{\dot{f}_{rot}}{\text{Hz/s}}\right]^{1/2}\left[\frac{\text{Hz}}{f_{rot}}\right]^{1/2} \tag{4}$$

where I_{38} is the star's moment of inertia in units of 10^{38}kg m^2. Different values of the moment of inertia are possible according to the NS equation of state, mass and spin[31], however in this work we will assume its canonical value to be $I = 10^{38}\text{kg m}^2$. The corresponding spin-down limit on the star's equatorial fiducial ellipticity can be obtained from Eq. (3):

$$\epsilon_{sd} = 1.91 \times 10^5\,I_{38}^{-1/2}\left[\frac{\dot{f}_{rot}}{\text{Hz/s}}\right]^{1/2}\left[\frac{\text{Hz}}{f_{rot}}\right]^{5/2}. \tag{5}$$

which does not depend on the star's distance.

B. The 5-vector narrowband pipeline

The narrow-band pipeline uses the 5-vector method [32] and, in particular, its latest implementation for narrow-band searches described in [33].

The pipeline explores a range of frequency and spin-down values by applying barycentric and spin-down corrections to the data, and then identifies the GW signal using its characteristic frequency components.

The pipeline firstly removes the modulations given by the barycentric corrections and intrinsic source spin-down. The barycentric corrections are applied using a frequency-independent non-uniform resampling [33]. The spin-down is removed by applying a phase correction on the data time series. Also the Einstein delay is corrected in the time domain.

Once we have removed the barycentric and spin-down modulations of a possible signal, the GW signal power is spread among five frequencies, given by the coupling of the signal frequency and the detector sidereal responses $A_+(t), A_\times(t)$. These frequency components are: $f_{gw} - 2F_{sid}$, $f_{gw} - F_{sid}$, f_{gw}, $f_{gw} + F_{sid}$ and $f_{gw} + 2F_{sid}$, where F_{sid} is the frequency corresponding to the Earth sidereal day.

Hence a pair of matched filters, one for each sidereal response function, is computed for each point of the explored parameter space. This is done using a frequency grid which allows us to compute the matched filters simultaneously over the whole analyzed frequency band. These steps are done separately for each detector. Then, the output of the matched filters, at each point of the parameter space, are combined, taking into account the phase shift[1] between the two data sets, in order to build a detection statistic.

The next step consists in selecting the maximum of the detection statistic for every 10^{-4} Hz interval and over the whole spin-down range. Within this set, points in the parameter space with a p-value below a 0.1% threshold (taking into account the number of trials) are considered potentially interesting outliers and are subject to further analysis steps, see App. B for more details.

III. THE ANALYSIS

The LIGO second observing run O2 started on November 30th 2016 16:00:00 UTC and ended on August 25th 2017 22:00:00 UTC, while Virgo joined the run later, on August 1st 2017 12:00:00 UTC, and ended on August 25th 2017 22:00:00 UTC. The narrow-band search can be performed jointly between different detectors if the data sets cover the same observing time. Since Virgo O2 data covered just ∼1 month at the end of O2, and was characterized by a lower sensitivity with respect to LIGO data, we have decided to exclude it from the analysis. For this analysis we have used the second version of calibratated LIGO data (C02) [34]. We jointly analyzed LIGO Hanford (LHO) and LIGO Livingston (LLO) data over the period between January 4th 2017 00:00:00 UTC and August 25th 2017 22:00:00 UTC. LLO data between the beginning of the run and December 22th 2016 have been excluded due to bad spectral contamination,

while both detectors underwent a commissioning break between December 22th 2016 and January 4th 2017. The observing time T_{obs} was ∼ 232 days, implying frequency and spin-down bins of, respectively, $\delta f = 5 \times 10^{-8}$ Hz and $\delta \dot{f} = 2.5 \times 10^{-15}$ Hz/s. LHO and LLO duty cycles were about 45% and the 56% and corresponded to an effective observing time of 104 days and 129 days respectively[2]. The sensitivity of the O2 search is reported in Fig. 1, where we show also O1 sensitivity. While at lower frequency only O2 LLO seems to be much better than O1, at higher frequencies the sensitivity is significantly better for both the detectors. In order to validate the analysis, we have looked for 4 hardware injections in the data checking if their parameters were recovered correctly, see Appendix A.

The explored frequency and spindown ranges were set to 0.4% of the pulsar rotational frequency and spindown reported in the ephemeris. Since in this analysis we subsampled data at 1 Hz, the explored frequency region of some pulsars has been chosen manually in order to avoid a possible signal aliasing.

We have decided to select as *outliers* for the follow-up the points in the parameter space with a value of the detection statistic corresponding to a p-value of 0.1% (taking into account the number of trials) or smaller. In the previous O1 search we used a threshold of 1%, due to the fact that data quality of LHO and LLO was significantly different at lower frequencies, see Appendix B for more details.

IV. SELECTED TARGETS

In our O2 analysis we have selected as an initial set of targets all the pulsars present in the O1 narrow-band search[27]. Then we have enlarged it, deciding to analyze all the pulsars with rotation frequency of 10 Hz and 350 Hz with spin-down limit, given in Eq. (4), within a factor 10 from the optimal sensitivity of the search of O2 LLO (in most cases). This choice has been driven by the fact that available pulsar distances can be affected by a large error. The spindown limit has been computed according to the most recent estimation of the distance given in the ATNF catalog[35] (*v1.58*) and extrapolating the rotational frequency and spindown rate at the O2 epoch. For the pulsars: J1028−5819, J1112−6103, J1813−1246 and J2043+2740, we have checked that the extrapolated rotational parameters together with the ranges explored in the narrow-band search covers the values reported by the updated ephemeris during the O2 epoch in [19]. While for the pulsars J0835−4510, J0940−5428, J1105−6107, J1410−6132, J1420−6048, J1531−5610, J1718−3825, J1809−1917 and J1838−0655

———

[1] This is given by the fact that the data sampling usually does not begin at the exact same time for different detectors.

———

[2] With the exception of pulsars that have glitched during the analysis. For those we have performed two independent analysis before and after the glitch.
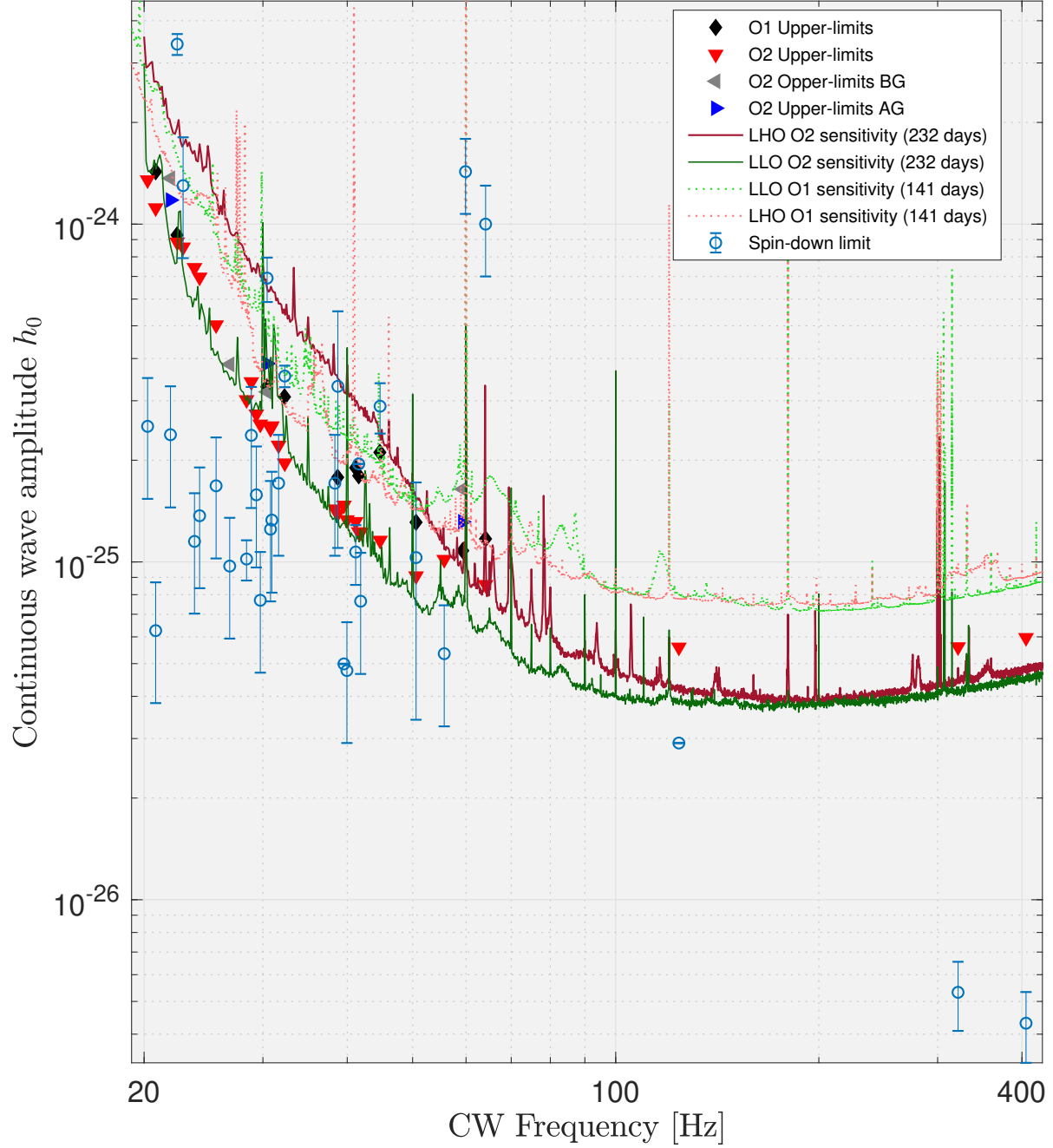
FIG. 1. *Vertical axis:* CW amplitude, *horizontal axis:* searched GW frequencies. The different lines indicate the estimated search sensitivity for O1 and O2 narrow-band searches, while the different markers indicate ULs. The labels "AG" and " BG" refers to a search performed after or before the glitch of a given pulsar. The error bars correspond to the uncertainties on the pulsar distance and correspond to 1σ confidence level.

the extrapolated spin-down rate resulted off-range with respect to the one reported in [19] and for this reason searched parameter space has been adjusted in such a way to cover the updated values. For the pulsars J0205+6449, J0534+2200, J1913+1011, J1952+3252 and J2229+6114 we have used updated ephemerides provided by the telescopes at Jodrell Bank (UK). For the remaining pulsars, no monitoring is present during the O2 run. Even though we are aware that an extrapolation from outdated ephemerides might bring to a GW search which does not cover the actual pulsar rotational parameters during O2, we have decided to carry on the analysis in such a way to exploit the possibility that the actual pulsar rotational parameters were covered even partially by the narrow-band search.

Tab. I reports the spindown limit on amplitude h_0 and ellipticity ϵ for each target, given their distance estimation and uncertainty. Hereafter, the distance uncertainties are propagated to the derived quantities (such as the spin-down limit) assuming normal distributions, namely:

$$\sigma_Y^2 = \left(\frac{\partial Y}{\partial d}\right)^2 \sigma_d^2,$$

with Y being a function of the distance and σ^2 the distribution variance.

The spindown limits are compared to the estimated narrow-band search sensitivity in Fig 1. The analysis covers the 11 targets that we have already analyzed for O1 plus 22 new targets. Based on the estimated sensitivity we expected to surpass the spin-down limit, in the O2 analysis, for 9 of the 11 O1 targets. The exceptions are J2043+2740 and J2229+6114, for which the current distance estimation has been increased with respect to the ATNF catalog *v1.54* (the catalog used for O1 [27]).

The new O2 targets mainly consist of pulsars with rotational frequencies within 10 Hz and 20 Hz with spindown rate $< -10^{-12}$ Hz/s, but there are also a few millisecond pulsars, for which we can approach the spindown limit. Among these there is the millisecond pulsar J2124+3358, for which we expect to barely approach the spin-down limit with targeted searches. One of these millisecond pulsars, J1300+1240, is located in a binary system. However, according to the orbital parameters in the ephemeris, the intrinsic binary orbital modulation on a possible CW signal would be of the order of $\Delta f_{\rm bin} \approx 10^{-10}$ Hz, that is below our frequency resolution and hence can be neglected[3]. Millisecond pulsars are characterized by a low rotational spindown value $\dot{f}_{\rm rot}$ together with a high rotational frequency $f_{\rm rot}$, hence according to Eq. (4), also their spindown limit will be harder to surpass by our search sensitivities. Although the narrow-band search is currently not sensitive enough for the millisecond pulsars, we have decided to perform

―――――――

[3] The frequency shift due to the binary motion has been computed using [50].

TABLE I. Properties of analyzed pulsars. The second column reports the distance as provided by the ephemerides, based on the dispersion measure and the Galactic electron density model of [36]. If the pulsar distance is estimated according to an independent measure, this is referred next to the name entry. The distance uncertainty refers to 1σ confidence level and is assumed to have a normal distribution. In the third and fourth column the spin-down limit $h_{\rm sd}$ and the corresponding ellipticity $\epsilon_{\rm sd}$ are computed using Eqs. (4)-(5).

Name	d [kpc]	$h_{\rm sd}$	$\epsilon_{\rm sd}$
J0205+6449[37]	2.0 ± 0.3	$(6.9 \pm 1.1) \cdot 10^{-25}$	$1.42 \cdot 10^{-3}$
J0534+2200[38]	2.0 ± 0.5	$(1.4 \pm 0.4) \cdot 10^{-24}$	$7.56 \cdot 10^{-4}$
J0537−6910[39]	49.7 ± 0.2	$(2.91 \pm 0.02) \cdot 10^{-26}$	$8.90 \cdot 10^{-5}$
J0540−6919[39]	49.7 ± 0.2	$(4.99 \pm 0.02) \cdot 10^{-26}$	$1.50 \cdot 10^{-3}$
J0835−4510[40]	0.28 ± 0.02	$(3.4 \pm 0.3) \cdot 10^{-24}$	$1.80 \cdot 10^{-3}$
J0940−5428	0.4 ± 0.2	$(1.3 \pm 0.5) \cdot 10^{-24}$	$8.97 \cdot 10^{-4}$
J1028−5819	1.4 ± 0.6	$(2.4 \pm 1.0) \cdot 10^{-25}$	$6.70 \cdot 10^{-4}$
J1105−6107	2.4 ± 0.9	$(1.7 \pm 0.7) \cdot 10^{-25}$	$3.82 \cdot 10^{-4}$
J1112−6103	4.5 ± 1.8	$(1.3 \pm 0.5) \cdot 10^{-25}$	$5.61 \cdot 10^{-4}$
J1300+1240[41]	0.7 ± 0.2	$(5.3 \pm 1.3) \cdot 10^{-27}$	$3.17 \cdot 10^{-8}$
J1302−6350	2.3 ± 0.9	$(7.6 \pm 3.0) \cdot 10^{-26}$	$9.52 \cdot 10^{-5}$
J1400−6325[42]	0.9 ± 0.3	$(1.0 \pm 0.3) \cdot 10^{-24}$	$2.07 \cdot 10^{-4}$
J1410−6132	13.5 ± 5.3	$(4.8 \pm 1.9) \cdot 10^{-26}$	$3.83 \cdot 10^{-4}$
J1420−6048	5.6 ± 2.2	$(1.6 \pm 0.7) \cdot 10^{-25}$	$9.81 \cdot 10^{-4}$
J1524−5625	3.4 ± 1.3	$(1.7 \pm 0.7) \cdot 10^{-25}$	$8.25 \cdot 10^{-4}$
J1531−5610	2.8 ± 1.1	$(1.2 \pm 0.5) \cdot 10^{-25}$	$5.47 \cdot 10^{-4}$
J1617−5055	4.7 ± 1.9	$(2.4 \pm 1.0) \cdot 10^{-25}$	$1.28 \cdot 10^{-3}$
J1718−3825	3.5 ± 1.4	$(9.7 \pm 3.8) \cdot 10^{-26}$	$4.48 \cdot 10^{-4}$
J1747−2809	8.2 ± 3.2	$(1.7 \pm 0.7) \cdot 10^{-25}$	$8.97 \cdot 10^{-4}$
J1747−2958	2.5 ± 1.0	$(2.5 \pm 1.0) \cdot 10^{-25}$	$1.47 \cdot 10^{-3}$
J1809−1917	3.3 ± 1.3	$(1.4 \pm 0.6) \cdot 10^{-25}$	$7.27 \cdot 10^{-4}$
J1811−1925	5.0 ± 2.0	$(1.3 \pm 0.6) \cdot 10^{-25}$	$6.59 \cdot 10^{-4}$
J1813−1246[43]	> 2.5	$< 1.9 \cdot 10^{-25}$	$2.67 \cdot 10^{-4}$
J1813−1749[44]	4.7 ± 0.8	$(2.9 \pm 0.5) \cdot 10^{-25}$	$6.42 \cdot 10^{-4}$
J1831−0952	3.7 ± 1.5	$(7.7 \pm 3.0) \cdot 10^{-26}$	$3.04 \cdot 10^{-4}$
J1833−1034[45]	4.1 ± 0.3	$(3.6 \pm 0.3) \cdot 10^{-25}$	$1.32 \cdot 10^{-3}$
J1838−0655[46]	6.6 ± 0.9	$(1.0 \pm 0.2) \cdot 10^{-25}$	$7.94 \cdot 10^{-4}$
J1913+1011	4.6 ± 1.8	$(5.4 \pm 2.1) \cdot 10^{-26}$	$7.54 \cdot 10^{-5}$
J1952+3252[41]	3.0 ± 2.0	$(1.0 \pm 0.7) \cdot 10^{-25}$	$1.15 \cdot 10^{-4}$
J2022+3842[47]	10.0 ± 2.0	$(1.1 \pm 0.3) \cdot 10^{-25}$	$6.00 \cdot 10^{-4}$
J2043+2740	1.5 ± 0.6	$(6.3 \pm 2.5) \cdot 10^{-26}$	$2.03 \cdot 10^{-4}$
J2124−3358[48]	0.4 ± 0.1	$(4.3 \pm 1.0) \cdot 10^{-27}$	$9.49 \cdot 10^{-9}$
J2229+6114[49]	3.0 ± 2.0	$(3.3 \pm 2.3) \cdot 10^{-25}$	$6.27 \cdot 10^{-4}$

the search in order to test the capabilities of the pipeline at higher frequencies.

Furthermore, pulsars J0205+6449, J0534+2200, J0835-4510,J1028−5819 and J1718−3825 had a glitch during O2. J0205+6449 glitched on May 27th 2017, J0534+2200 glitched on Mar 27th 2017, J0835-4510 had a glitch on Dec 16th 2016 [51], J1028−5819 glitched on May 29th 2017 and J1718−3825 glitched on May 1st July 2017 [19]. For these pulsars we have performed

two independent analyses, one before and one after the glitch, excluding the day in which the glitch was present. For J0835-4510 and J1718−3825 only the analysis after or before the glitch has been done, since few data were available before or after the two glitches.

Tab. II reports the frequency/spin-down regions that we have analyzed for each of the 33 targets. The reference time for the rotational parameters of the pulsars is December 1 2016 00:00:00 UTC.

V.   RESULTS

The search has produced a total of 49 outliers for 15 of the 33 targets. Every outlier underwent a chain of follow-up steps aimed to test its nature, namely: *i)* check for the presence of known instrumental noise lines, *ii)* comparing the SNR GW amplitude estimation among several detectors and *iii)* studying the outlier significance with software injections. The outliers are given in Tab. III together with the step of the follow-up where we excluded them.

The narrow-band search carried out in the past on O1 data [27] produced two interesting outliers for J0835−4510 and 1833−1034. In order to confirm or reject them, the data from the first four months of O2 (available with calibration version C01 at the time) were used and no evidence for a signal was found. The full O2 analysis discussed in this paper confirms those findings. No outlier has been found for J0835−4510, while an outlier has been found for J1833−1034, at a slightly different frequency which however, as discussed in the next section, has been vetoed.

A.   Outliers follow-up

The first step of the follow-up was to check if a known instrumental noise line was present in one of the two detectors [52]. This ruled out most of the candidates for the pulsars J1105−6107 and J2121−3358, see Appendix C for more details.

The second step of the follow-up was to study the evolution of the recovered signal-to-noise ratio (SNR) and amplitude h_0 with respect to the fraction of data samples that we are integrating. We expect the SNR to increase as the square root of the integration time and the amplitude h_0 to be nearly constant. We have performed this type of test in a LHO, LLO and joint search for different integration times, checking if the SNR and h_0 estimation were compatible across the different cases.

Many outliers at frequencies < 100 Hz have been classified as LHO disturbances, since they have been observed only in LHO (see Appendix C). Some of these are in proximity of unidentified noise lines (lines which are confidently classified as detector disturbances, but whose origin is unknown). That is the case of the outliers from

J1112−6103, J1302−6350 and J1813−1246. Other outliers at low frequency were not in proximity of unidentified noise lines but have been vetoed as the signal-to-noise ratio is bigger than 8 only in LHO data, which has a sensitivity 2 to 3 times worse than LLO, thus being incompatible with a true CW signal.

Only 3 outliers survived up to the third step of the follow-up, namely from pulsars J1300+1240, J1617−5055 and J2124−3358. For all these pulsars we cannot approach the theoretical spin-down limit with our current search sensitivity, and this is a strong hint for the noise origin of these outliers. The last step of the follow-up consisted in studying the SNR and recovered CW amplitude h_0 with software injections with an amplitude h_0 fixed to that estimated for the outlier. The evolution of the SNR and h_0 for the outlier is then compared to the distributions derived from the injections. If they are compatible among the three different analyses, LHO, LLO and joint combination, the outlier is subject to more dedicated studies. The two remaining outliers for the millisecond pulsars were ruled out since they were present in just one detector, while the injections predicted that they would be visible in both the detectors. The J1617−5055 remaining outlier were also ruled out, as the injections show that they were likely driven by an LHO disturbance. Refer to Appendix C for more details on the last steps of this follow-up.

B.   Upper limits

Since there was no evidence for the presence of a CW signal, we have computed upper limits (ULs) on the CW amplitude h_0. The ULs have been produced using the same procedure as in the O1 narrow-band search [27], which consists in injecting non-overlapping GW signals with fixed amplitude h_0 in data every 10^{-4} Hz intervals. When the 95% of injections produce a value of the detection statistic higher than the one used for the outlier selection, we set the upper-limit to the injected amplitude value.

Fig. 1 shows the median value of the UL for each of the 33 targets. The ULs are driven at lower frequencies by LLO sensitivity, since it is the most sensitive detector in that frequency region. On the other hand, at higher frequencies the ULs lie close to the sensitivity of the two detectors, which are indeed similar.

Tab. IV summarizes our results for the O2 narrow-band search. The table reports the median value of the UL on the strain amplitude h_0 and the corresponding ellipticity, computed using Eq. (5). We consider the spin-down limit surpassed for a given pulsar, if the ULs are lower than the spin-down limit over the entire frequency band.

The most stringent ULs have been set for the 3 pulsars J0537−6910, J1300+1240 and J2124−3358 and are of the order of 5.5×10^{-26} which, however, are above the spin-down limit. The lowest ellipticity UL has been set for

TABLE II. First column: pulsar name. Second and third columns: central frequency and frequency width explored in the search. Fourth and fifth columns: central spin-down and spin-down ranges explored in the search. Sixth and seventh column: number of templates in frequency and spin-down. Frequency and spin-down resolutions are, respectively, $\delta f \sim 5 \times 10^{-8}$ Hz, $\delta \dot{f} \sim 2.5 \times 10^{-15}$ Hz/s. The labels "AG" and "BG" indicate, respectively, after and before the glitch. Note that the frequency and spin-down resolution, and hence the number of templates, is lower in the case of pulsars with a glitch.

Name	f [Hz]	Δf [Hz]	$\dot{f}$ [Hz/s]	$\Delta \dot{f}$ [Hz/s]	$n_f [10^6]$	$n_{\dot{f}}$
J0205+6449 AG	30.41	0.06	$-8.61 \cdot 10^{-11}$	$2.72 \cdot 10^{-13}$	0.47	17
J0205+6449 BG	30.41	0.06	$-8.61 \cdot 10^{-11}$	$2.44 \cdot 10^{-13}$	0.74	37
J0534+2200 AG	59.30	0.12	$-7.38 \cdot 10^{-10}$	$1.50 \cdot 10^{-12}$	1.53	251
J0534+2200 BG	59.30	0.12	$-7.38 \cdot 10^{-10}$	$1.56 \cdot 10^{-12}$	0.82	75
J0537−6910	123.86	0.25	$-3.92 \cdot 10^{-10}$	$8.01 \cdot 10^{-13}$	4.95	321
J0540−6919	39.39	0.08	$-3.71 \cdot 10^{-10}$	$7.56 \cdot 10^{-13}$	1.57	303
J0835−4510	22.37	0.04	$-3.22 \cdot 10^{-11}$	$8.51 \cdot 10^{-14}$	0.89	35
J0940−5428	22.84	0.05	$-8.56 \cdot 10^{-12}$	$2.50 \cdot 10^{-14}$	0.91	11
J1028−5819 AG	21.88	0.04	$-3.86 \cdot 10^{-12}$	$3.56 \cdot 10^{-14}$	0.33	3
J1028−5819 BG	21.88	0.04	$-3.86 \cdot 10^{-12}$	$2.63 \cdot 10^{-14}$	0.54	5
J1105−6107	31.64	0.06	$-7.94 \cdot 10^{-12}$	$2.00 \cdot 10^{-14}$	1.26	9
J1112−6103	30.78	0.06	$-1.49 \cdot 10^{-11}$	$3.50 \cdot 10^{-14}$	1.23	15
J1300+1240	321.62	0.64	$-5.91 \cdot 10^{-15}$	$5.00 \cdot 10^{-15}$	12.86	3
J1302−6350	41.87	0.08	$-2.00 \cdot 10^{-12}$	$5.00 \cdot 10^{-15}$	1.67	3
J1400−6325	64.12	0.13	$-8.00 \cdot 10^{-11}$	$1.65 \cdot 10^{-13}$	2.56	67
J1410−6132	39.95	0.08	$-2.52 \cdot 10^{-11}$	$7.01 \cdot 10^{-14}$	1.60	29
J1420−6048	29.32	0.06	$-3.57 \cdot 10^{-11}$	$1.00 \cdot 10^{-13}$	1.17	41
J1524−5625	25.56	0.05	$-1.27 \cdot 10^{-11}$	$3.00 \cdot 10^{-14}$	1.02	13
J1531−5610	23.75	0.05	$-3.88 \cdot 10^{-12}$	$1.50 \cdot 10^{-14}$	0.95	7
J1617−5055	28.80	0.06	$-5.62 \cdot 10^{-11}$	$1.15 \cdot 10^{-13}$	1.15	47
J1718−3825 BG	26.78	0.05	$-4.72 \cdot 10^{-12}$	$1.72 \cdot 10^{-14}$	0.82	5
J1747−2809	38.32	0.08	$-1.14 \cdot 10^{-10}$	$2.35 \cdot 10^{-13}$	1.53	95
J1747−2958	20.23	0.04	$-1.25 \cdot 10^{-11}$	$3.00 \cdot 10^{-14}$	0.81	13
J1809−1917	24.17	0.05	$-7.44 \cdot 10^{-12}$	$2.00 \cdot 10^{-14}$	0.97	9
J1811−1925	30.91	0.06	$-2.10 \cdot 10^{-11}$	$4.50 \cdot 10^{-14}$	1.23	19
J1813−1246	41.60	0.08	$-1.52 \cdot 10^{-11}$	$3.50 \cdot 10^{-14}$	1.66	15
J1813−1749	44.71	0.09	$-1.27 \cdot 10^{-10}$	$2.60 \cdot 10^{-13}$	1.79	105
J1831−0952	29.73	0.06	$-3.67 \cdot 10^{-12}$	$1.00 \cdot 10^{-14}$	1.19	5
J1833−1034	32.29	0.06	$-1.05 \cdot 10^{-10}$	$2.15 \cdot 10^{-13}$	1.29	87
J1838−0655	28.36	0.06	$-1.99 \cdot 10^{-11}$	$5.51 \cdot 10^{-14}$	1.13	23
J1913+1011	55.69	0.11	$-5.25 \cdot 10^{-12}$	$1.50 \cdot 10^{-14}$	2.23	7
J1952+3252	50.59	0.10	$-7.48 \cdot 10^{-12}$	$2.00 \cdot 10^{-14}$	2.02	9
J2022+3842	41.16	0.08	$-7.30 \cdot 10^{-11}$	$1.50 \cdot 10^{-13}$	1.64	61
J2043+2740	20.80	0.04	$-2.75 \cdot 10^{-13}$	$5.00 \cdot 10^{-15}$	0.83	3
J2124−3358	405.59	0.81	$-16.92 \cdot 10^{-16}$	$5.00 \cdot 10^{-15}$	16.21	3
J2229+6114	38.71	0.08	$-5.84 \cdot 10^{-11}$	$1.20 \cdot 10^{-13}$	1.55	49

TABLE III. This table summarizes the outliers found in the O2 narrowband search. The first column reports the name of the pulsar for which we have found outliers. The second column gives the central frequency of the pulsar search band and the third column the p-value of the least significant outlier. The last column reports the step of the follow-up in which we have vetoed the outliers. For a description of the follow-up steps refer to the main text.

Name	f	num cand.	p-value	Step
J1105−6107	31.64	16[a]	4.23×10^{-4}	i,ii
J1112−6103	30.78	1[b]	1.83×10^{-4}	ii
J1300+1240	321.62	1	7.80×10^{-4}	iii
J1302−6350	41.87	4[c]	7.79×10^{-4}	ii
J1420−6048	29.32	11[d]	9.82×10^{-4}	i,ii
J1531−5610	23.75	1	4.65×10^{-4}	ii
J1617−5055	28.80	2	7.80×10^{-4}	ii,iii
J1747−2809	38.32	1	9.68×10^{-4}	ii
J1811−1925	30.91	1	3.30×10^{-4}	ii
J1813−1246	41.60	2[e]	6.73×10^{-4}	ii,iii
J1831−0952	29.73	1	2.15×10^{-4}	ii
J1833−1034	32.29	1	9.33×10^{-4}	ii
J1952+3252	50.59	4[f]	4.48×10^{-4}	i,ii
J2124−3358	405.59	2[g]	5.61×10^{-4}	i,iii
J2229+6114	38.71	1	9.66×10^{-4}	ii

[a] most vetoed since they are close to the comb line of 0.987925 Hz comb in LLO and comb line of 2.109223 Hz in LHO.
[b] Various unidentified lines around 35.51 Hz.
[c] Unidentified noise disturbance in LHO at 41.8838 Hz.
[d] Comb of 1.945501 Hz in LHO.
[e] Unidentified broad line disturbance at 41.654-41.660 Hz.
[f] comb of 2.109223 Hz in LHO, comb of 1.9455045 Hz in LHO, comb of 1.945437 Hz in LHO.
[g] Comb of 0.9967943 Hz in LLO.

J1300+1240, of about 3.3×10^{-7}. We have been able to surpass the spin-down limit for the pulsars: J0205+6449, J0534+2200 (Crab), J0835−4510 (Vela), J1400−6325, J1813−1246 (assuming the lower bound for the distance), J1813−1749, J1833−1034 and J2229+6114. For J0940−5428, while the median value of the UL is below the spin-down limit, a small fraction of the individual results are above. For J1747−2809 and J1952+3252 we are close to surpassing the spin-down limit[4], see Tab. IV. For all the pulsars for which we have surpassed the spin-down limit, we have computed the upper limit on the ratio of the GW to the rotational energy loss. The lower ULs on the GW energy loss are for J0534+2200 and J1400−6325, corresponding to a fraction of about 0.8%. The lowest ULs on the GW amplitude and ellipticity among the pulsars for which we have surpassed the spin-down limit are, respectively, 8.29×10^{-26} and 1.78×10^{-5}, for J1400−6325. For a canonical pulsar with a radius of about 10 km, this number would correspond to a maximum surface deformation of about 5 cm.

For the remaining 22 targets we were not able to surpass the spin-down limit. Tab. IV roughly suggests to us that an improvement in sensitivity of a factor 3 is needed for most of the low-frequency pulsars. It must be considered, however, that the spin-down limits have been computed assuming a canonical value for the moment of inertia of $10^{38} \mathrm{kg\,m^2}$. In fact, it could be significantly larger, depending on NS equation of state, up to $\sim 3 \times 10^{38} \mathrm{kg\,m^2}$, implying a spin-down limit $\sim \sqrt{(3)}$ times larger.

VI. CONCLUSION

Overall, the narrow-band search over O2 data has brought an improvement with respect to previous searches in terms of ULs. On the other hand, ULs are similar to those found in O1 for pulsars with rotation frequency below 30 Hz. For instance the UL on the Vela pulsar (around 22 Hz) has improved by 10%, while the UL on J0205+6449[5] has improved by about 22%. On the other hand for pulsars with expected GW frequencies > 30 Hz the UL is improved even by a factor 2. The UL on J0534+2200 did not improve, since in O2 we split the analysis in two different chunks due to the presence of the glitch. For this reason the UL, both before and after the glitch, is comparable with the one found in O1 analysis. We have also been able to surpass the spin-down limit for two pulsars that were not analyzed in O1, J0940−5428, J1747−2809.

We are still not able to surpass the spin-down limit for the millisecond pulsars and for low frequency pulsars with spin-down below $\sim 10^{-12}$ Hz/s. However, we are able to surpass the spin-down limit for low frequency and high energetic pulsars (such as Crab or J1833−1034) or for low frequency pulsars that are close to the Earth.

---

[4] Excluding a frequency band heavily contaminated by noise.

---

[5] Please note that the spin-down limit of this pulsar has been computed using two different distance in O1 and O2. For O1 we used 2.0 kpc [54] while for O2 the nominal ephemeris value was 3.2 kpc.

TABLE IV. Upper limits summary table. First column: pulsar name. Second and third columns: median of the 95% confidence level UL on the GW amplitude h_0 and corresponding ellipticity ϵ. Fourth column: surface deformation corresponding to the median ellipticity for a NS with radius of 10 km [53]. Fifth column: ratio between the median UL and the spin-down limit. Sixth column: ratio between the median UL on the GW and rotational energy losses. Last column: minimum and maximum ratio between the ULs and the theoretical spin-down limit over the analyzed frequency/spindown region. All the entries that use information on the astrophysical distance also include the corresponding uncertainty at 1σ confidence level.

Name	$\langle h \rangle_{\mathrm{UL}}$	$\langle \epsilon \rangle_{\mathrm{UL}}$	r_ϵ[cm]	$\langle h \rangle_{\mathrm{UL}}/h_{\mathrm{sd}}$	$\langle \dot{E}_{\mathrm{UL}}\rangle/\dot{E}_{\mathrm{sd}}$	$\min_{\mathrm{nb}}[\langle h \rangle_{\mathrm{UL}}/h_{\mathrm{sd}}] - \max_{\mathrm{nb}}[\langle h \rangle_{\mathrm{UL}}/h_{\mathrm{sd}}]$
J0205+6449 AG	$3.87 \cdot 10^{-25}$	$(7.9 \pm 1.2) \cdot 10^{-4}$	197.9	0.56 ± 0.08	0.3	$0.48^{+0.07}_{-0.07} - 0.67^{+0.10}_{-0.10}$
J0205+6449 BG	$3.19 \cdot 10^{-25}$	$(6.5 \pm 1.0) \cdot 10^{-4}$	163.1	0.46 ± 0.07	0.2	$0.31^{+0.05}_{-0.05} - 0.58^{+0.09}_{-0.09}$
J0534+2200 AG	$1.31 \cdot 10^{-25}$	$(7.1 \pm 1.8) \cdot 10^{-5}$	17.4	0.09 ± 0.02	0.008	$0.07^{+0.02}_{-0.02} - 0.11^{+0.03}_{-0.03}$
J0534+2200 BG	$1.64 \cdot 10^{-25}$	$(8.8 \pm 2.2) \cdot 10^{-5}$	21.7	0.11 ± 0.03	0.01	$0.09^{+0.02}_{-0.02} - 0.14^{+0.03}_{-0.03}$
J0537−6910	$5.59 \cdot 10^{-26}$	$(1.7 \pm 0.01) \cdot 10^{-4}$	-	1.92 ± 0.01	-	$1.13^{+0.00}_{-0.00} - 2.25^{+0.01}_{-0.01}$
J0540−6919	$1.47 \cdot 10^{-25}$	$(4.43 \pm 0.02) \cdot 10^{-3}$	-	2.95 ± 0.01	-	$1.83^{+0.01}_{-0.01} - 3.47^{+0.02}_{-0.02}$
J0835−4510	$8.82 \cdot 10^{-25}$	$(4.7 \pm 0.4) \cdot 10^{-4}$	116.8	0.26 ± 0.02	0.07	$0.14^{+0.01}_{-0.01} - 0.31^{+0.02}_{-0.02}$
J0940−5428	$8.55 \cdot 10^{-25}$	$(5.9 \pm 2.3) \cdot 10^{-4}$	147.6	0.7 ± 0.3	0.5	$0.4^{+0.2}_{-0.2} - 0.8^{+0.4}_{-0.4}$
J1028−5819 AG	$1.18 \cdot 10^{-24}$	$(3.3 \pm 1.3) \cdot 10^{-3}$	-	5.0 ± 2.0	-	$4.2^{+1.7}_{-1.7} - 6.0^{+2.3}_{-2.3}$
J1028−5819 BG	$1.37 \cdot 10^{-24}$	$(3.8 \pm 1.5) \cdot 10^{-3}$	-	5.7 ± 2.3	-	$4.3^{+1.7}_{-1.7} - 7.0^{+2.7}_{-2.7}$
J1105−6107	$2.20 \cdot 10^{-25}$	$(5.0 \pm 2.0) \cdot 10^{-4}$	123.0	1.3 ± 0.6	1.7	$0.68^{+0.3}_{-0.3} - 1.88^{+0.8}_{-0.8}$
J1112−6103	$2.48 \cdot 10^{-25}$	$(1.1 \pm 0.5) \cdot 10^{-3}$	-	2.0 ± 0.8	-	$1.1^{+0.5}_{-0.5} - 2.5^{+1.0}_{-1.0}$
J1300+1240	$5.60 \cdot 10^{-26}$	$(3.3 \pm 0.8) \cdot 10^{-7}$	-	10.5 ± 2.5	-	$6.3^{+1.5}_{-1.5} - 13.1^{+3.1}_{-3.1}$
J1302−6350	$1.22 \cdot 10^{-25}$	$(1.5 \pm 0.6) \cdot 10^{-4}$	38.0	1.6 ± 0.7	2.6	$0.7^{+0.3}_{-0.3} - 1.9^{+0.8}_{-0.8}$
J1400−6325	$8.57 \cdot 10^{-26}$	$(1.8 \pm 0.6) \cdot 10^{-5}$	4.4	0.09 ± 0.03	0.008	$0.05^{+0.01}_{-0.01} - 0.10^{+0.03}_{-0.03}$
J1410−6132	$1.33 \cdot 10^{-25}$	$(1.1 \pm 0.5) \cdot 10^{-3}$	-	2.8 ± 1.1	-	$1.4^{+0.6}_{-0.6} - 3.5^{+1.4}_{-1.4}$
J1420−6048	$2.75 \cdot 10^{-25}$	$(1.7 \pm 0.7) \cdot 10^{-3}$	426.8	1.7 ± 0.7	3.1	$0.9^{+0.4}_{-0.4} - 2.2^{+0.9}_{-0.9}$
J1524−5625	$5.03 \cdot 10^{-25}$	$(2.5 \pm 1.0) \cdot 10^{-3}$	-	3.0 ± 1.2	-	$1.7^{+0.7}_{-0.7} - 3.7^{+1.5}_{-1.5}$
J1531−5610	$7.51 \cdot 10^{-25}$	$(3.6 \pm 1.4) \cdot 10^{-3}$	-	6.5 ± 2.6	-	$3.7^{+1.5}_{-1.5} - 7.7^{+3.1}_{-3.1}$
J1617−5055	$3.41 \cdot 10^{-25}$	$(1.8 \pm 0.6) \cdot 10^{-3}$	461.0	1.5 ± 0.6	2.1	$0.8^{+0.3}_{-0.3} - 1.8^{+0.8}_{-0.8}$
J1718−3825 BG	$3.88 \cdot 10^{-25}$	$(1.8 \pm 0.7) \cdot 10^{-3}$	-	4.0 ± 1.6	-	$2.5^{+1.0}_{-1.0} - 4.8^{+2.0}_{-2.0}$
J1747−2809	$1.43 \cdot 10^{-25}$	$(7.5 \pm 2.9) \cdot 10^{-4}$	188.1	0.8 ± 0.4	0.6	$0.5^{+0.2}_{-0.2} - 1.0^{+0.4}_{-0.4}$
J1747−2958	$1.35 \cdot 10^{-24}$	$(7.9 \pm 3.1) \cdot 10^{-3}$	-	5.4 ± 2.1	-	$3.2^{+1.3}_{-1.3} - 6.7^{+2.6}_{-2.6}$
J1809−1917	$6.95 \cdot 10^{-25}$	$(3.7 \pm 1.5) \cdot 10^{-3}$	-	5.1 ± 2.0	-	$3.1^{+1.2}_{-1.2} - 6.2^{+2.4}_{-2.4}$
J1811−1925	$2.53 \cdot 10^{-25}$	$(1.2 \pm 0.5) \cdot 10^{-3}$	-	1.9 ± 0.8	-	$1.3^{+0.5}_{-0.5} - 2.3^{+0.9}_{-0.9}$
J1813−1246	$1.23 \cdot 10^{-25}$	$\leq 7 \cdot 10^{-4}$	42.0	≥ 0.7	≥ 0.5	$\geq (0.4 - 0.8)$
J1813−1749	$1.16 \cdot 10^{-25}$	$(2.6 \pm 0.5) \cdot 10^{-4}$	64.5	0.40 ± 0.07	0.2	$0.25^{+0.04}_{-0.04} - 0.49^{+0.08}_{-0.08}$
J1831−0952	$2.56 \cdot 10^{-25}$	$(1.0 \pm 0.4) \cdot 10^{-3}$	-	3.3 ± 1.3	-	$2.1^{+0.9}_{-0.9} - 4.2^{+1.7}_{-1.7}$
J1833−1034	$1.96 \cdot 10^{-25}$	$(7.3 \pm 0.6) \cdot 10^{-4}$	182.5	0.55 ± 0.04	0.3	$0.35^{+0.03}_{-0.03} - 0.71^{+0.05}_{-0.05}$
J1838−0655	$3.03 \cdot 10^{-25}$	$(2.4 \pm 0.4) \cdot 10^{-3}$	-	3.0 ± 0.4	-	$1.8^{+0.3}_{-0.3} - 3.6^{+0.5}_{-0.5}$
J1913+1011	$1.02 \cdot 10^{-25}$	$(1.4 \pm 0.6) \cdot 10^{-4}$	-	1.9 ± 0.8	-	$1.1^{+0.5}_{-0.5} - 2.31^{+0.9}_{-0.9}$
J1952+3252	$9.09 \cdot 10^{-26}$	$(1.0 \pm 0.7) \cdot 10^{-4}$	25.2	0.9 ± 0.6	0.8	$0.5^{+0.4}_{-0.4} - 1.1^{+0.8}_{-0.8}$
J2022+3842	$1.32 \cdot 10^{-25}$	$(7.4 \pm 1.5) \cdot 10^{-4}$	184.0	1.2 ± 0.3	1.4	$0.7^{+0.2}_{-0.2} - 1.5^{+0.3}_{-0.3}$
J2043+2740	$1.12 \cdot 10^{-24}$	$(3.6 \pm 1.4) \cdot 10^{-3}$	-	17.8 ± 7.0	-	$10.3^{+4.0}_{-4.0} - 21.42^{+9.0}_{-9.0}$
J2124−3358	$5.97 \cdot 10^{-26}$	$(1.3 \pm 0.3) \cdot 10^{-7}$	-	14.0 ± 3.3	-	$7.3^{+1.8}_{-1.8} - 17.4^{+4.2}_{-4.2}$
J2229+6114	$1.39 \cdot 10^{-25}$	$(2.7 \pm 1.8) \cdot 10^{-4}$	65.8	0.4 ± 0.3	0.2	$0.3^{+0.2}_{-0.2} - 0.5^{+0.4}_{-0.4}$

Appendix A: Validation with hardware injections

Hardware injections are simulated signals in LIGO-Virgo data for testing purposes. These artificial signals are injected by a control system which acts on the mirror and simulate a CW signal. The Hardware injections are continuously monitored and their injected parameters are known. In order to validate the efficiency of the pipeline used in this paper, we have looked for 4 Hardware injections in LIGO data studying the accuracy of

TABLE V. Accuracy of the parameter estimation for the O2 hardware injections. The first three columns report the name, frequency and spin-down of the hardware injections (reference time at Dec 1st 2017 UTC 00:00:00). The last three columns report the relative errors in percentage for the parameter estimation. The relative errors are defined in the text.

Name	$f_{\rm gw}$ [Hz]	$\dot{f}_{\rm gw}$ [Hz/s]	ϵ_{h_0}	ϵ_η	ϵ_ψ
Pulsar 2	575.16	$-1.37 \cdot 10^{-13}$	6%	0.3%	-
Pulsar 3	108.86	$-1.46 \cdot 10^{-17}$	0.01%	0.3%	2%
Pulsar 5	52.81	$-4.03 \cdot 10^{-18}$	3%	0.07%	1%
Pulsar 8	190.46	$-8.65 \cdot 10^{-9}$	8%	0.03%	0.07%

the recovered parameters. We define the relative error on the CW amplitude recovery as $\epsilon_{h_0} = 1 - h_0^{\rm esti}/h_0^{\rm inj}$, where $h_0^{\rm inj}$ is the injected CW amplitude and $h_0^{\rm esti}$ is the recovered value. Whereas we define the relative error on the angular parameters ψ, η as $\epsilon_\psi = |\psi^{\rm inj} - \psi^{\rm esti}|/90\deg$ and $\epsilon_\eta = |\eta^{\rm inj} - \eta^{\rm esti}|/2$. Tab. V reports the errors on the parameter estimation for the validation tests performed with the O2 hardware injections.

Appendix B: validation of the threshold

The narrow-band search is based on the 5-vector method [29], that was implemented originally for *targeted searches*. In that context just one template is explored for each detector, and an overall threshold on the p-value of, say, 1% for the candidate selection is sufficient to efficiently recover 95% of injected signals with SNR=8. However, in narrow-band searches we are exploring a large number of templates in a frequency region of about 0.04 Hz or more, using two detectors that have different data quality, i.e. different level of noise and duty cycle. The threshold in this case is computed by using as noise background the values of the statistic excluded from the local maxima selection and then extrapolating the long tails of the distribution. By definition, these excluded points are representative of the noise level in the given frequency bands. This means that, if the noise level in the 10^{-4} Hz wide frequency sub-band that we are analyzing is slightly higher than the noise level in the overall frequency region from which we are generating noise backgrounds, then close-to-threshold outliers will occur. These close-to-threshold outliers may be not completely distinguishable from the actual noise. As an example, we have generated 200 software injections with amplitude h_0 fixed to the one that generated a 1% p-value outlier in the post-glitch analysis of pulsar J0534+2200. We have estimated the recovered signal-to-noise ratio of the injections by integrating coherently more and more data from LHO and LLO. If the injections are distinguishable from the noise, we expect 95% of the injections to have a recovered signal-to-noise ratio greater than 8. However, it is shown by Fig. 2 this is not the case. For a full coherent
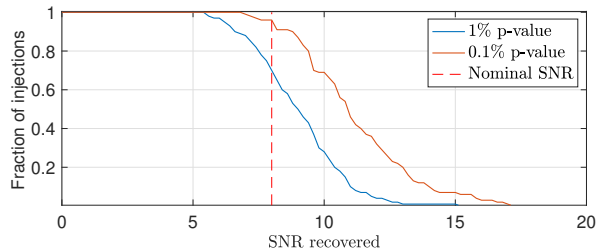
FIG. 2. *Vertical axis:* fraction of injections recovered with an SNR equal or higher than the one indicated on the *horizontal axis.* The different line colors indicate a set of software injections that would produce an outlier at 1% and 0.1% according to the evaluation of the noise-only distribution of the detection statistic. The red-dashed vertical line indicates the SNR=8 threshold that is commonly used to distinguish the signal from the noise.

LHO-LLO search, the distribution of the recovered SNR is below 8. We have also performed the same test by injecting fake signals with an amplitude h_0 that would correspond to a 0.1% outlier. In this case, as shown in Fig. 2, the recovered SNR of the injections is higher than 8, confirming that the 0.1% p-value threshold represents a more conservative choice while recovering CW signals.

Appendix C: Follow-up test cases

We report in this appendix some explanatory plots of the analysis steps used for outliers follow-up. The first step consisted in checking if a known noise line was present in the proximity of the outlier. We considered an outlier consistent with a known noise disturbance if it is found in a frequency region covered by the frequency variation of the noise line due to the Doppler and spindown corrections.

Many of the outliers found in the case of the pulsar J1105−6107 and J1952+3252 originated from vetoed combs in one or both of the detectors. Fig. 3 and Fig. 4 show the spectra of the time series obtained for J1105−6107 and J1952+3252 outliers. In the first case, noise combs pollute both LLO and LHO, while in the second case different noise combs contribute to the same noise disturbance at 50.58 Hz in LHO data.

The second step of the follow-up chain was to study the evolution of the recovered CW amplitude h_0 and the recovered SNR of the outlier with respect to the integration time. In Fig. 5 we report the recovered SNR for different integration times. In this frequency region, the LHO noise floor is about two times higher than the LLO noise floor. Hence in the presence of a reliable CW outlier, we would expect the recovered SNR to be higher in LLO and the joint analysis. As shown in Fig. 5, this is not the case and the outlier is probably due to an unknown noise disturbance in LHO.

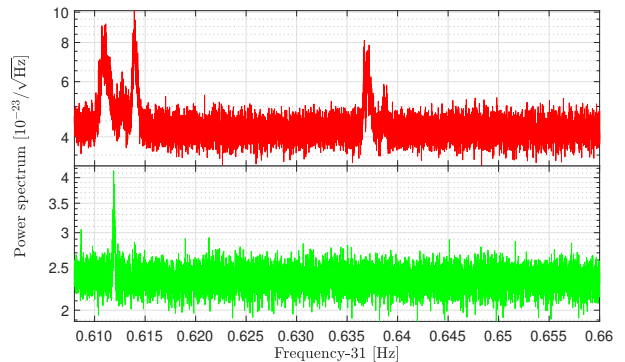The last step of the follow-up consisted in studying the

FIG. 3. *Top*: LHO spectrum around the expected frequency of J1105−6107. *Bottom*: LLO spectrum around the expected signal frequency of J1105−6107. In both the detectors, we see the contribution of various noise lines which are known comb with fundamental frequency 0.987925 Hz in LLO and 2.109223 Hz in LHO.
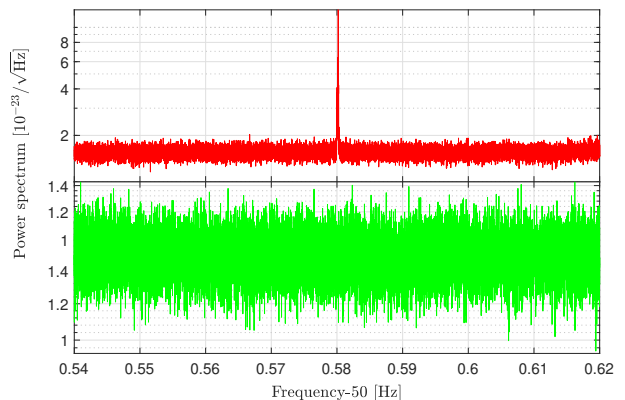

FIG. 4. *Top*: LHO spectrum around the expected frequency of J1952+3252. *Bottom*: LLO spectrum around the expected frequency of J1952+3252. In LHO we see the contribution of various noise lines due to combs with fundamental frequencies 2.109223 Hz, 1.9455045 Hz and 1.945437 in LHO.

noise properties with software injections around the candidates. The software injections had amplitude h_0 equal to the one recovered from the most sensitive search. This corresponds to LLO for most of the frequencies < 40 Hz, while it is the joint search if the noise floor of the two detectors is comparable. The recovered distribution of the CW amplitude and SNR for the software injections is then plotted with respect to the integration time of the analysis and compared with the recovered CW amplitude and SNR for the outlier. Fig. 6 shows the distributions of the recovered SNR and CW amplitude for 200 software injections with an amplitude fixed at $h_0 = 3.9 \times 10^{-26}$,
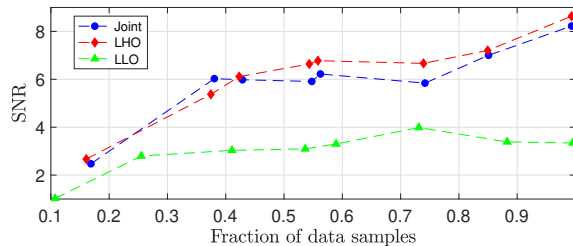
FIG. 5. Example of the first stage follow-up for one of the not candidates of J1105+6107 that were not vetoed. The recovered SNR of the outlier is on the vertical axis while the horizontal axis indicates the fraction of data samples that we are integrating with the matched filter. The outlier is visible only in LHO and propagates to the joint analysis.

which is the one recovered for the outlier of the millisec-

ond pulsar J1300+1240 in the joint search. The software injections have a frequency at least 10^{-3} Hz away from the actual outlier, in such a way to not interfere with the outlier. From Fig. 6 we can see that the outlier seems to be compatible with the results of the software injections in LLO data, but on the other hand it is not compatible with the joint and LHO analysis. In this frequency region, the detectors noise floor is similar and we would expect comparable results for the LLO and LHO analysis. The software injections show that a signal with amplitude $h_0 \approx 3.9 \times 10^{-26}$ would be distinguishable from the noise in the joint search because the recovered SNR of the software injections with the same amplitude for a joint full coherent search is always higher than 7.5. On the contrary, in the joint search the SNR of the actual outlier (black dashed line) is low and not compatible with the results of the software injections, suggesting that the outlier is due to a unknown noise disturbance present in LLO.

[1] The LIGO Scientific Collaboration and J. et al. Aasi. Advanced ligo. *Classical and Quantum Gravity*, 32(7):074001, 2015.

[2] The LIGO Scientific Collaboration, the Virgo Collaboration, and B. P. et al. Abbott. Gw150914: The advanced ligo detectors in the era of first discoveries. *Phys. Rev. Lett.*, 116:131103, Mar 2016.

[3] The Virgo Collaboration and F. a et al. Acernese. Advanced virgo: a second-generation interferometric gravitational wave detector. *Classical and Quantum Gravity*, 32(2):024001, 2015.

[4] The LIGO Scientific Collaboration, the Virgo Collaboration, and B. P. et al. Abbott. GWTC-1: A Gravitational-Wave Transient Catalog of Compact Binary Mergers Observed by LIGO and Virgo during the First and Second Observing Runs. *arXiv e-prints*, page arXiv:1811.12907, November 2018.

[5] The LIGO Scientific Collaboration, the Virgo Collaboration, and B. P. et al. Abbott. Observation of gravitational waves from a binary black hole merger. *Physical Review Letters*, 116(6):1–16, 2016.

[6] The LIGO Scientific Collaboration, the Virgo Collaboration, and B. P. et al. Abbott. GW151226: Observation of Gravitational Waves from a 22-Solar-Mass Binary Black Hole Coalescence. *Physical Review Letters*, 116(24):241103, jun 2016.

[7] The LIGO Scientific Collaboration, the Virgo Collaboration, and B. P. et al. Abbott. GW170814: A Three-Detector Observation of Gravitational Waves from a Binary Black Hole Coalescence. *Physical Review Letters*, 119(14):141101, oct 2017.

[8] The LIGO Scientific Collaboration, the Virgo Collaboration, and B. P. et al. Abbott. GW170104: Observation of a 50-Solar-Mass Binary Black Hole Coalescence at Redshift 0.2. *Physical Review Letters*, 118(22):221101, jun 2017.

[9] The LIGO Scientific Collaboration, the Virgo Collaboration, and B. P. et al. Abbott. GW170608: Observation of a 19-solar-mass Binary Black Hole Coalescence. 35, 2017.

[10] The LIGO Scientific Collaboration, the Virgo Collaboration, and B. P. et al. Abbott. GW170817: Observation of Gravitational Waves from a Binary Neutron Star Inspiral. *Physical Review Letters*, 119(16):161101, oct 2017.

[11] The LIGO Scientific Collaboration and B. P. et al. Abbott. Setting upper limits on the strength of periodic gravitational waves from PSR J1939+2134 using the first science data from the GEO 600 and LIGO detectors. *Phys. Rev. D*, 69(8):082004, April 2004.

[12] B. P. et al. The LIGO Scientific Collaboration Abbott. Limits on Gravitational-Wave Emission from Selected Pulsars Using LIGO Data. *Physical Review Letters*, 94(18):181103, May 2005.

[13] The LIGO Scientific Collaboration, the Virgo Collaboration, and B. P. et al. Abbott. Upper limits on gravitational wave emission from 78 radio pulsars. *Phys. Rev. D*, 76(4):042001, August 2007.

[14] The LIGO Scientific Collaboration, the Virgo Collaboration, and B. P. et al. Abbott. Beating the Spin-Down Limit on Gravitational Wave Emission from the Crab Pulsar. *The Astrophysical Journal Letters*, 683:L45, August 2008.

[15] The LIGO Scientific Collaboration, the Virgo Collaboration, and B. P. et al. Abbott. Searches for Gravitational Waves from Known Pulsars with Science Run 5 LIGO Data. *Astrophys. J.*, 713:671–685, April 2010.

[16] The LIGO Scientific Collaboration, the Virgo Collaboration, and J. et al. Abadie. Beating the Spin-down Limit on Gravitational Wave Emission from the Vela Pulsar. *Astrophys. J.*, 737:93, August 2011.

[17] The LIGO Scientific Collaboration, the Virgo Collaboration, and J. et al. Aasi. Gravitational Waves from Known Pulsars: Results from the Initial Detector Era. *Astrophys. J.*, 785:119, April 2014.

[18] The LIGO Scientific Collaboration, the Virgo Collaboration, and B. P. et al. Abbott. First Search for Gravitational Waves from Known Pulsars with Advanced LIGO. *Astrophys. J.*, 839:12, April 2017.
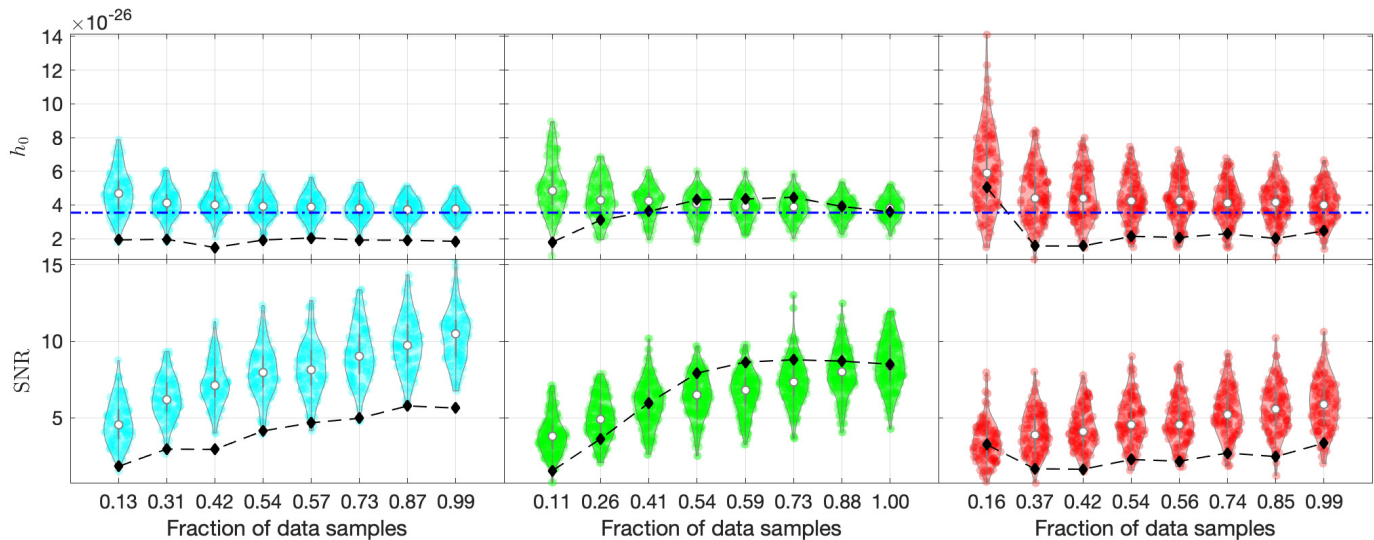
FIG. 6. These plots show the distribution of the recovered CW amplitude h_0 and SNR for 200 software injections in the frequency region around the outlier of the millisecond pulsar J1300+1240. The black dashed line indicates the observed estimator for the outlier. *First and second rows of plots*: Recovered CW amplitude and SNR. *First, second and third columns of plots:* Joint, LLO and LHO searches.

[19] The LIGO Scientific Collaboration, the Virgo Collaboration, and B. P. et al. Abbott. Searches for Gravitational Waves from Known Pulsars at Two Harmonics in 2015-2017 LIGO Data. 2019.

[20] The LIGO Scientific Collaboration, the Virgo Collaboration, and J. et al. Aasi. Searches for Continuous Gravitational Waves from Nine Young Supernova Remnants. *Astrophys. J.*, 813:39, November 2015.

[21] The LIGO Scientific Collaboration, the Virgo Collaboration, and B. P. et al. Abbott. Searches for Continuous Gravitational Waves from Fifteen Supernova Remnants and Fomalhaut b with Advanced LIGO. *arXiv e-prints*, December 2018.

[22] The LIGO Scientific Collaboration, the Virgo Collaboration, and J. et al. Aasi. Directed search for gravitational waves from Scorpius X-1 with initial LIGO data. *Phys. Rev. D*, 91(6):062008, March 2015.

[23] The LIGO Scientific Collaboration, the Virgo Collaboration, B. P. Abbott, and Abbott et al. Search for gravitational waves from Scorpius X-1 in the first Advanced LIGO observing run with a hidden Markov model. *Phys. Rev. D*, 95(12):122003, June 2017.

[24] The LIGO Scientific Collaboration, the Virgo Collaboration, and B. P. et al. Abbott. Upper Limits on Gravitational Waves from Scorpius X-1 from a Model-based Cross-correlation Search in Advanced LIGO Data. *Astrophys. J.*, 847:47, September 2017.

[25] The LIGO Scientific Collaboration, the Virgo Collaboration, and B. P. et al. Abbott. First search for nontensorial gravitational waves from known pulsars. *Phys. Rev. Lett.*,

120:031104, Jan 2018.

[26] The LIGO Scientific Collaboration, the Virgo Collaboration, and J. et al. Aasi. Narrow-band search of continuous gravitational-wave signals from Crab and Vela pulsars in Virgo VSR4 data. *Phys. Rev. D*, 91(2):022004, January 2015.

[27] The LIGO Scientific Collaboration, the Virgo Collaboration, and B. P. et al. Abbott. First narrow-band search for continuous gravitational waves from known pulsars in advanced detector data. *Phys. Rev. D*, 96(12):122006, December 2017.

[28] D. I. Jones and N. Andersson. Gravitational waves from freely precessing neutron stars. *Monthly Notices of the Royal Astronomical Society*, 331(1):203–220, 2002.

[29] P. Astone, S. D'Antonio, S. Frasca, and C. Palomba. A method for detection of known sources of continuous gravitational wave signals in non-stationary data. *Classical and Quantum Gravity*, 27(19):194016, October 2010.

[30] P. Jaranowski, A. Królak, and B. F. Schutz. Data analysis of gravitational-wave signals from spinning neutron stars: The signal and its detection. *Phys. Rev. D*, 58(6):063001, September 1998.

[31] M. Bejger. Parameters of rotating neutron stars with and without hyperons. *Astronomy & Astrophysics*, 552:A59, April 2013.

[32] P. Astone, A. Colla, S. D'Antonio, S. Frasca, C. Palomba, and R. Serafinelli. Method for narrow-band search of continuous gravitational wave signals. *Phys. Rev. D*, 89(6):062008, March 2014.

[33] S. Mastrogiovanni, P. Astone, S. D'Antonio, S. Frasca,

G. Intini, P. Leaci, A. Miller, C. Palomba, O. J. Piccinni, and A. Singhal. An improved algorithm for narrow-band searches of continuous gravitational waves. *Classical and Quantum Gravity*, 34(13):135007, July 2017.

[34] C. Cahillane, J. Betzwieser, D. A. Brown, E. Goetz, E. D. Hall, K. Izumi, S. Kandhasamy, S. Karki, J. S. Kissel, G. Mendell, R. L. Savage, D. Tuyenbayev, A. Urban, A. Viets, M. Wade, and A. J. Weinstein. Calibration uncertainty for Advanced LIGO's first and second observing runs. *Phys. Rev. D*, 96(10):102001, November 2017.

[35] R. N. Manchester, G. B. Hobbs, A. Teoh, and M. Hobbs. The Australia Telescope National Facility Pulsar Catalogue. *The Astronomical Journal*, 129:1993–2006, April 2005.

[36] J. M. Yao, R. N. Manchester, and N. Wang. A New Electron-density Model for Estimation of Pulsar and FRB Distances. *Astrophys. J.*, 835:29, January 2017.

[37] R. Kothes. Distance and age of the pulsar wind nebula 3C 58. *Astronomy & Astrophysics*, 560:A18, December 2013.

[38] D. L. Kaplan, S. Chatterjee, B. M. Gaensler, and J. Anderson. A Precise Proper Motion for the Crab Pulsar, and the Difficulty of Testing Spin-Kick Alignment for Young Neutron Stars. *Astrophys. J.*, 677:1201–1215, April 2008.

[39] G. Pietrzyński, D. Graczyk, W. Gieren, I. B. Thompson, B. Pilecki, A. Udalski, I. Soszyński, S. Kozłowski, P. Konorski, K. Suchomska, G. Bono, P. G. P. Moroni, S. Villanova, N. Nardetto, F. Bresolin, R. P. Kudritzki, J. Storm, A. Gallenne, R. Smolec, D. Minniti, M. Kubiak, M. K. Szymański, R. Poleski, Ł. Wyrzykowski, K. Ulaczyk, P. Pietrukowicz, M. Górski, and P. Karczmarek. An eclipsing-binary distance to the Large Magellanic Cloud accurate to two per cent. *Nature (London)*, 495:76–79, March 2013.

[40] R. Dodson, D. Legge, J. E. Reynolds, and P. M. McCulloch. The Vela Pulsar's Proper Motion and Parallax Derived from VLBI Observations. *Astrophys. J.*, 596:1137–1141, October 2003.

[41] J. P. W. Verbiest, J. M. Weisberg, A. A. Chael, K. J. Lee, and D. R. Lorimer. On Pulsar Distance Measurements and Their Uncertainties. *Astrophys. J.*, 755:39, August 2012.

[42] M. Renaud, V. Marandon, E. V. Gotthelf, J. Rodriguez, R. Terrier, F. Mattana, F. Lebrun, J. A. Tomsick, and R. N. Manchester. Discovery of a Highly Energetic Pulsar Associated with IGR J14003-6326 in the Young Uncataloged Galactic Supernova Remnant G310.6-1.6. *Astrophys. J.*, 716:663–670, June 2010.

[43] M. Marelli, A. Harding, D. Pizzocaro, A. De Luca, K. S. Wood, P. Caraveo, D. Salvetti, P. M. Saz Parkinson, and F. Acero. On the Puzzling High-Energy Pulsations of the Energetic Radio-Quiet γ-Ray Pulsar J1813-1246. *Astrophys. J.*, 795:168, November 2014.

[44] J. P. Halpern, E. V. Gotthelf, and F. Camilo. Spin-down Measurement of PSR J1813-1749: The Energetic Pulsar Powering HESS J1813-178. *The Astrophysical Journal Letters*, 753:L14, July 2012.

[45] F. Camilo, S. M. Ransom, B. M. Gaensler, P. O. Slane, D. R. Lorimer, J. Reynolds, R. N. Manchester, and S. S. Murray. PSR J1833-1034: Discovery of the Central Young Pulsar in the Supernova Remnant G21.5-0.9. *Astrophys. J.*, 637:456–465, January 2006.

[46] E. V. Gotthelf and J. P. Halpern. Discovery of a Young, Energetic 70.5 ms Pulsar Associated with the TeV Gamma-Ray Source HESS J1837-069. *Astrophys. J.*, 681:515–521, July 2008.

[47] P. Arumugasamy, G. G. Pavlov, and O. Kargaltsev. XMM-Newton Observations of Young and Energetic Pulsar J2022+3842. *Astrophys. J.*, 790:103, August 2014.

[48] G. Desvignes, R. N. Caballero, L. Lentati, J. P. W. Verbiest, D. J. Champion, B. W. Stappers, G. H. Janssen, P. Lazarus, S. Osłowski, S. Babak, C. G. Bassa, P. Brem, M. Burgay, I. Cognard, J. R. Gair, E. Graikou, L. Guillemot, J. W. T. Hessels, A. Jessner, C. Jordan, R. Karuppusamy, M. Kramer, A. Lassus, K. Lazaridis, K. J. Lee, K. Liu, A. G. Lyne, J. McKee, C. M. F. Mingarelli, D. Perrodin, A. Petiteau, A. Possenti, M. B. Purver, P. A. Rosado, S. Sanidas, A. Sesana, G. Shaifullah, R. Smits, S. R. Taylor, G. Theureau, C. Tiburzi, R. van Haasteren, and A. Vecchio. High-precision timing of 42 millisecond pulsars with the European Pulsar Timing Array. *MNRAS*, 458:3341–3380, May 2016.

[49] J. P. Halpern, F. Camilo, E. V. Gotthelf, D. J. Helfand, M. Kramer, A. G. Lyne, K. M. Leighly, and M. Eracleous. PSR J2229+6114: Discovery of an Energetic Young Pulsar in the Error Box of the EGRET Source 3EG J2227+6122. *The Astrophysical Journal Letters*, 552:L125–L128, May 2001.

[50] P. Leaci and R. Prix. Directed searches for continuous gravitational waves from binary systems: Parameter-space metrics and optimal Scorpius X-1 sensitivity. *Phys. Rev. D*, 91(10):102003, May 2015.

[51] J. Palfreyman, J. M. Dickey, A. Hotan, S. Ellingsen, and W. van Straten. Alteration of the magnetosphere of the Vela pulsar during a glitch. *Nature (London)*, 556:219–222, April 2018.

[52] P. B. Covas, A. Effler, E. Goetz, P. M. Meyers, A. Neunzert, M. Oliver, B. L. Pearlstone, V. J. Roma, R. M. S. Schofield, V. B. Adya, and et al. Identification and mitigation of narrow spectral artifacts that degrade searches for persistent gravitational waves in the first two observing runs of Advanced LIGO. *Phys. Rev. D*, 97(8):082002, April 2018.

[53] Nathan K. Johnson-McDaniel. Gravitational wave constraints on the shape of neutron stars. *Phys. Rev. D*, 88(4):044016, Aug 2013.

[54] R. Kothes. Distance and age of the pulsar wind nebula 3C 58. *Astronomy & Astrophysics*, 560:A18, December 2013.